12-15-2007

Magnetic and Transport Properties of Oxide Thin Films

Yuanjia Hong
University of New Orleans

Magnetic and Transport Properties of Oxide Thin Films

A Dissertation

Submitted to the Graduate Faculty of the
University of New Orleans
in partial fulfillment of the
requirements for the degree of

Doctor of Philosophy
in
Engineering and Applied Science

by

Yuanjia Hong

M.S. Changchun Institute of Optic and Fine Mechanics, ChangChun, P.R.China, 2000

December 2007

ACKNOWLEDGEMENTS

This dissertation was funded in part by Sharp Laboratories of America and by Louisiana Board of Regents Support Fund Grant No. LEQSF(2004-07)-RD-B-12.

I would like to say first and foremost what an honor to receive the guidance of Dr. Jinke Tang. He provided me the opportunity to come to the United States to work on my degree through the offer of an assistantship to work in his research group. Through the years, he has shown me keen academic insight, and great patience, and has shared his extensive acknowledge both in and beyond science. His wise guidance has helped shape my career and my life.

It has been an enjoyable learning experience to work with my Committee members Dr. Carl Ventrice, Dr. Rasheed M. A. Azzam, Dr. Ashok Puri and Dr. Kevin Stokes. I am sincerely grateful for all their time and assistance. I also would like to thank Dr. Leszek Malkinski for serving on my general exam committee.

I would like to thank the following for their experimental expertise, and the use of their equipment in my research: Dr Leonard Spinu, Dr. John B. Wiley, and Dr. Weilei Zhou. I also learned considerably from Dr. Wendong Wang, Dr. Zhenjun Wang. I would like to thank Dr. Hongguo Zhang, Dr. Minghui Yu, Dr. Gabriel Caruntu, Mr. Cosmin Radu, Mr. Jiajun Chen and Mr. Renhai Long for their assistance in my experimental work.

I would like to thank Ms. Pat Robbert for sharing her experience and countless interesting and stimulating discussions.

Thanks to Dr. C. Greg Seab, Dr. George Ioup and Dr. Juliette Ioup, who took the time to help and guide me in the PhD program, and were supportive over the years. Thank you to Mr. N.B. Day, Ms Sandra Merz, and Ms.Zella Huaracha for handling all of the innumerable daily

challenges of keeping the department running smoothly, including all the extra help involved with an international student.

I have more than usual thankfulness that I would like to express for assistance given during the difficult period after Hurricane Katrina.

To Tao Fang, Chairman of the LSU Chinese Student and Scholar Association, along with his wife Tao Yang, for the best care to student evacuees from new Orleans.

To Dr. Jeffery M. Gillespic and his wife Ms. Michelle Gillespie, who generously shared their sweet home with me and other evacuees after Katrina.

To Dashun Xue, Rong Zheng, and other classmates for the generosity to a guest student at LSU after Hurricane Katrina

To Ms. Pat Robbert and Dr. Stanley Goldberg who provided me a home while I was awating a FEMA trailer.

Thank you to the many friends I have met at UNO.

Thank you to Dr. Ronald C. Miller and Dr. Weldon Wilson for making time in their busy schedules to help me polish my English.

Thank you to Dr. Stephen Michael Rodrigue, who always brings inspiration and encouragement to me; he helped me through many difficulties along the way of pursuing my PhD. His belief in me has allowed me to increase my self-confidence.

Thank you to my dearest family, Yachen Yuan and Guangyan Hong, the foundation of my life, love, sacrifice and dedication and I am eternally grateful for all of your love and guidance making this entire processs rich and fulfilling.

ABSTRACT

My dissertation research focuses on the investigation of the transport and magnetic properties of transition metal and rare earth doped oxides, particularly SnO_2 and HfO_2 thin films. Cr- and Fe-doped SnO_2 films were deposited on Al_2O_3 substrates by pulsed-laser deposition. X-ray-diffraction patterns (XRD) show that the films have rutile structure and grow epitaxially along the (101) plane. The diffraction peaks of Cr-doped samples exhibit a systematic shift toward higher angles with increasing Cr concentration. This indicates that Cr dissolves in SnO_2. On the other hand, there is no obvious shift of the diffraction peaks of the Fe-doped samples. The magnetization curves indicate that the Cr-doped SnO_2 films are paramagnetic at 300 and 5 K. The Fe-doped SnO_2 samples exhibit ferromagnetic behaviour at 300 and 5 K. Zero-field-cooled and field-cooled curves indicate super paramagnetic behavior above the blocking temperature of 100 K, suggesting that it is possible that there are ferromagnetic particles in the Fe-doped films.

It was found that a $Sn_{0.98}Cr_{0.02}O_2$ film became ferromagnetic at room temperature after annealing in H_2. We have calculated the activation energy and found it decreasing with the annealing, which is explained by the increased oxygen vacancies/defects due to the H_2 treatment of the films. The ferromagnetism may be associated with the presence of oxygen vacancies although AMR was not observed in the samples.

Pure HfO_2 and Gd-doped HfO_2 thin films have been grown on different single crystal substrates by pulsed laser deposition. XRD patterns show that the pure HfO_2 thin films are of single monoclinic phase. Gd-doped HfO_2 films have the same XRD patterns except that their diffraction peaks have a shift toward lower angles, which indicates that Gd dissolves in HfO_2.

Transmission electron microscopy images show a columnar growth of the films. Very weak ferromagnetism is observed in pure and Gd-doped HfO_2 films on different substrates at 300 and 5 K, which is attributed to either impure target materials or signals from the substrates. The magnetic properties do not change significantly with post deposition annealing of the HfO_2 films.

Keywords

SnO_2, HfO_2, pulsed laser deposition, thin film, epitaxial growth, magnetic thin films, ferromagnetic materials, transport properties.

CHAPTER 1

INTRODUCTION

1.1 Spintronics

Traditional silicon chips in computers and other electronic devices control the flow of electrical current by modifying the positive or negative charge of different parts of each tiny circuit. Spintronics is "Spin-based electronics". The idea is to use the electron's spin, as well as its charge in the devices. Spins can exist in one of two states-- “up” or “down”, and this quality can be exploited to build smaller (potentially on atomic scale) binary devices that are non-volatile, faster, and more robust and use less power than charge-current-based devices. Furthermore, because of its quantum nature, electron spin may exist not only in the “up” or “down” state but also in many intermediate states depending on the energy of the system. All these qualities hold the potential for what is in effect highly parallel commutating, which is the basis for the quantum computers.[1]

Spintronics is not science fiction; it is already used in modern computers. The most successful spintronic device up-to-date is the GMR spin valve. This device utilizes a layered structure of thin films of magnetic materials, which change its electrical resistance depending on applied magnetic field direction. In a spin valve, as shown in Fig. 1.1, one of the ferromagnetic layers is "pinned"(top layer in Fig. 1.1), so its magnetization direction remains fixed, the other ferromagnetic layer is "free" to change depend on the applied magnetic field. When the applied magnetic field aligns the magnetization vectors of the free layer and the pinned layer to the same

direction, the electrical resistance of the device reaches its lower level. On the other hand, when the applied external field causes the free layer magnetization vector to rotate in a direction antiparallel to the pinned layer magnetization vector, the electrical resistance of the device reach its higher level due to spin dependent scattering.

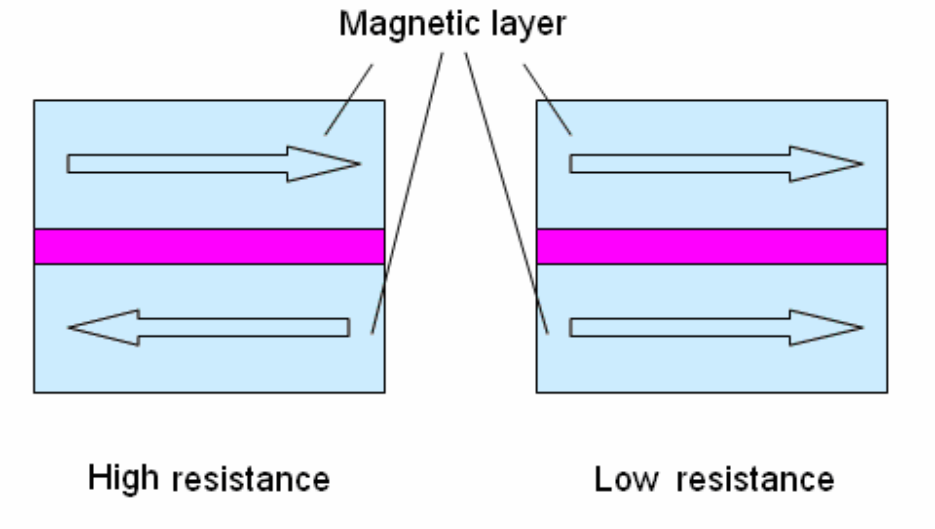

Fig. 1.1 Schematic diagram of spin valve.

GMR stands for giant magnetoresistance, it was independently discovered in 1988 in Fe/Cr/Fe trilayers by a research team led by Peter Grünberg of the Jülich Research Centre, who owns the patent[2], and in Fe/Cr multilayer by the group of Albert Fert of the University of Paris-Sud, who first saw the large effect in multilayer that led to its naming, and first correctly explained the underlying physics. The discovery of GMR is considered as the birth of spintronics and has earned both Grünberg and Fert the 2007 Nobel prize[3]. The primary advantage of GMR heads is greater sensitivity to magnetic fields from the disk. This increased sensitivity makes it possible to detect smaller recorded bits and to read these bits at higher data rates. Larger signals from GMR heads also help overcome electronic noise. GMR heads are expected to support area

densities beyond 11.6 Gbits/in².[4] The hard drive read heads in the current generation of computer hard drives utilize structures that consist of two layers of metallic ferromagnets (such as., Fe-Ni alloy) separated by a thin spacer layer (in the order of nm) of normal metal (such as Cr or Cu)[5]. The flow of current across the spacer layer is facilitated or inhibited depending on whether the magnetic moments of the two ferromagnets layers are parallel or anti-parallel to each other. Devices have been demonstrated with GMR ratios (i.e. the magnitude of the change, (Antiparallel Resistance - Parallel Resistance) / Parallel Resistance) as high as 60-70%.

Another success story of spintronics is room temperature tunnelling magnetoresistance (TMR), which was discovered in 1995 by Moodera et al[6]. When the normal metal layer in a spin valve is replaced by a thin insulator layer, electrons' tunnelling probability depends on the relative orientations of the two magnetic electrodes, and a very large TMR is achieved in such magnetic tunnel junctions). The discoveries help build up the foundation for a new generation of magnetic random access memory (MRAM)

1.2 Spintronics in Semiconductors --- Spin Injection

A modern computer chip contains many millions of tiny transistors; each acting as a tiny switch where a small current is used to control the flow of a larger current. Central to the success of modern electronics is the transistor. A transistor is a switch that controls the flow of electrical current.

The spin transistor utilizes both the spin and electronic characteristics of a conventional semiconductor transistor in combination with a carrier (current) flow controlled by magnetic moment to maximize gain.

Figure 1.2 below are schematic diagram of a spin transistor. Room temperature ferromagnetic semiconductor material will replace the n-type semiconductor both in the source (injector) and drain (collector) area. A spin injector can be occupied by spin polarized charge carriers with selected magnetic moment. In the collecting (drain) region, the electronic spins can be determined via application of an electric field, with the initial voltage applied on both the gate and the drain area, the current flow can be manipulated by the passing through or not via the magnetic barrier[7].

Unlike a normal electrical circuit that requires a continuous supply of power, these spin states are stable without necessarily requiring the application of an electric current, thus a spin transistor remains in the same magnetic state even when power is removed, which may lead to creating cost-effective non-volatile solid state storage device. It is one of the technologies being explored for Magnetic Random Access Memory (MRAM).

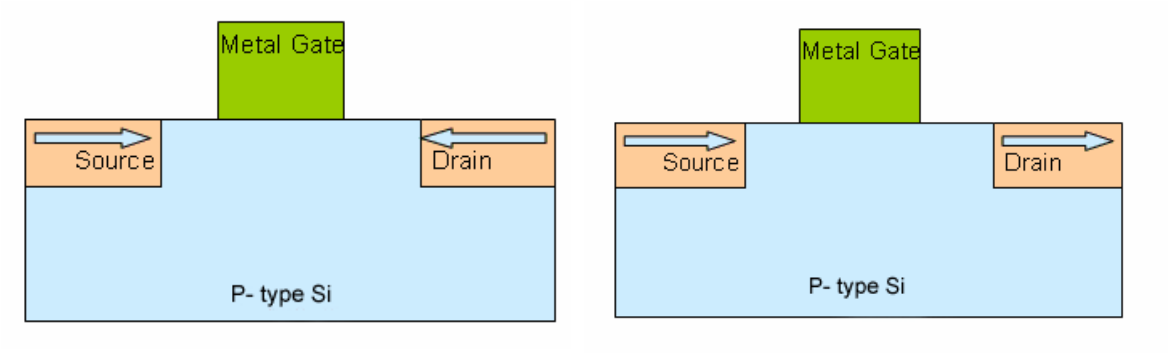

(a) (b)

Fig. 1.2 Schematic of a spin transistor.

The challenges to using spintronics for logic operations are so daunting. Not the least among them is finding the right material to build practical circuits. Remarkable progress has been made in recent years on all fronts. In particular, the plausibility of semiconductor spintronics has been bolstered by recent advances such as demonstration of coherent spin transport over macroscopic distances in a variety of semiconductors[8] and the discovery of a host of magnetic semiconductors[9]. However, there still have some challenge; such as (1) how to make spin injection from the ferromagnetic into the semiconductor as efficiently as possible, because the electrical current in the semiconductor injected from a ferromagnetic metal is consistently found to have minimum spin polarization. (2) What will be the mechanism of spin transport in semiconductors and spin detection?

Many approaches are being attempted to address these problems. From materials synthesis point of view, for example, the use of magnetic semiconductors with crystalline and electrical properties compatible with conventional semiconductors and with close to 100% spin polarization is encouraging. A promising group of materials are ferromagnetic oxides and related compounds, which are predicted to have 100%, spin polarization and referred to as "half-metals".[10] Interface engineering to generate non-diffusive transport such as tunnelling across the interface is another approach to enhance the spin injection into a semiconductor.

1.3 Half Metals

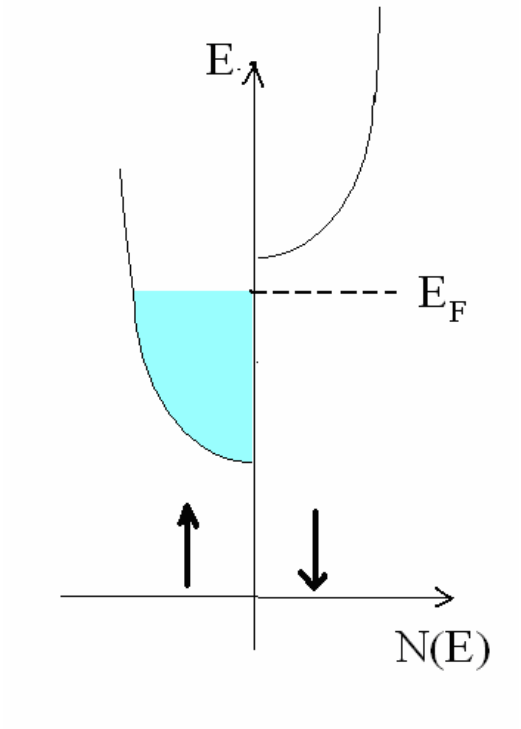

Fig. 1.3 Schematic densities of states N (E) for a magnetic semiconductor below T_c

The conduction of the spintronic devices, either spin-valve or first generation MRAM, depends firmly on the spin polarization of the ferromagnetic layers, and normally it is 40% in alloys such as Fe, Co, and Ni. Half metals[11] are ferromagnets with an unusual band structure and have only one type of conduction electron states at the Fermi level (E_F) shown in Fig. 1.3. Half-metals are 100% spin polarized based on theoretical calculation. Well-known half-metals include Fe_3O_4, CrO_2, Heusler alloys, and perovskite $La_{0.7}Sr_{0.3}MnO_3$.

1.4 Magnetic Semiconductors

Magnetic semiconductors are materials that exhibit both ferromagnetism and semiconductor properties. Whereas traditional electronics device are based on control of charge carriers (n-type or p-type), magnetic semiconductors would, in addition, allow control of spin states (up or down). What is interesting is that they would also provide 100% carrier spin polarization (thus behave much like a half-metal) in principle, which is important for spintronic applications, e.g., spin injection in spin FET as mentioned earlier.

An important class of magnetic semiconductor is dilute magnetic semiconductors (DMS), which are semiconductors doped with transition metals, i.e. electronically active elements. A few established III-V compound semiconductors such as GaAs become ferromagnetic when doped with 3-8% Mn[12], and their ferromagnetic transition temperatures can be well above 100 K[13]. These materials have been shown to act both as an acceptor and as a source of magnetic moment. Efforts to increase the critical temperatures up to room temperature is being intensively

pursued, but researchers still face challenges of understanding the fundamental limit on the transition temperature and the nature of the exchange coupling in these heavily doped materials.

A number of magnetic semiconductors are being currently investigated for their spintronic applications and the interesting physics involved in them. These include 1) II-VI, III-V and IV dilute semiconductors, 2) EuS and EuO, and 3) a host of doped oxide thin films.

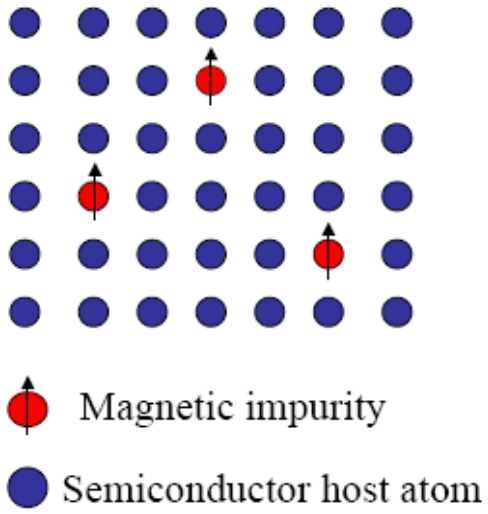

Fig. 1.4 Sketch of Ferromagnetic semiconductor

1.5 Oxide-diluted magnetic semiconductors

Based on the results of local density approximation of density function theory[14], oxide-diluted magnetic semiconductors (O-DMS) have attracted great interest in recent years due to the possibility of inducing room temperature ferromagnetism in certain oxides by transition metal doping. The report of room temperature ferromagnetism (FM) in Co:TiO_2 oxide[15] films has high lighted the experimental studies. Significant efforts were made to grow these doped oxides of high quality, pulsed laser deposition (PLD) and molecular beam epitaxy (MBE) have been used

to synthesis the thin film form due to the non-equilibrium process. Various systems with interesting properties (for example, high Curie temperature and large magnetic monent) have been obtained. Table I lists Properties of selected dilute magnetic semiconductor oxide thin films.

TABLE I. Properties of selected dilute magnetic semiconductor oxide thin films

Oxide	E_g (eV)	Dopant	M (μ_B/dopant)	T_c(K)	Reference
TiO_2	3.2	V --5%	4.2	>400	Hong et al (2004)
		Co--7%	1.4	>650	Sinde et al (2003)
		Fe --6 %	2.4	300	Wang et al (2003)
SnO_2	3.5	Fe --5 %	1.8	610	Coey et al (2004)
		Co--5%	7.5	650	Ogale et al (2003)
		Mn—0.3%	20		Coey (2005)
ZnO	3.3	V—15%	0.5	>350	Saeld et al (2001)
		Mn—2.2%	0.16	>300	P. Sharma et al (2003)
		Co—10%	2.0	280-300	Ueda et al (2001)
		Ni---0.9%	0.06	>300	Radovanovic et al (2003)
Cu_2O	2.0	Co—5%, Al –0.5%	0.2	>300	Kale et al (2003)

These O-DMS share interesting common features such as: 1) O-DMS are made by doping non-magnetic oxide with transition metals. 2) The oxides are either n-type or p-type

semiconductors. 3) The Curie temperature T_c of the O-DMSs can be far above room temperature. 4) O-DMS are mainly thin films of thickness around 10-300 nm fabricated by non-equilibrium processes.

There also some tasks we need to fulfil, such as: 1) Confirming room temperature ferromagnetism in materials. 2) Achieving desirable characteristics for spintronic applications. 3) Looking for empirical rules of the ferromagnetism. 4) Fabricating "new" materials.

The following topics will be discussed in the following chapters.

In Chapter 3, the procedure for synthesis Cr and Fe-doped SnO_2 by PLD is described. X-ray diffraction patterns indicate that Cr dissolves into SnO_2. The magnetization curves indicate that the Cr-doped SnO_2 films are completely paramagnetic. The Fe-doped SnO_2 samples are ferromagnetic at 300^{o}K and 5^{o}K. Zero-field-cooled (ZFC) and field-cooled (FC) curves indicate there are ferromagnetic particles in the films which behave superparamagnetically above the blocking temperature of about 100^{o}K. The anisotropic magnetoresistance effect was not observed in the Fe-doped SnO_2 samples.

In Chapter 4, the procedure for synthesis $Sn_{0.98}Cr_{0.02}O_2$ magnetic semiconductors is described. Composition analysis and XRD patterns indicated that Cr element was incorporated into SnO_2. The room temperature ferromagnetism with high magnetization was obtained after H_2 treatment of the film. In this system, local Cr atoms may establish long range ferromagnetic structure through sp-d interaction and local ferromagnetic structure through direct d-d exchange interaction between the neighbouring Cr atoms.

In Chapter 5, I discuss the structure and magnetic properties of pure and Gd-doped HfO_2 powders and thin films. HfO_2 powders (with and without annealing in H_2 flow) are not

ferromagnetic. For Gd-doped (3%) HfO_2 film, XRD result implies that Gd dissolves in HfO_2. The film exhibits obvious paramagnetic signal at low temperature. ZFC-FC curves do not show ferromagnetic behaviour.

CHAPTER 2

EXPERIMENTAL TECHNIQUES

2.1 Introduction to Pulsed Laser Deposition

The main idea of pulsed laser deposition (PLD) derives from the laser material removal mechanism; PLD relies on the photon-material interaction to create an ejected plume of material from any target. The plasma (plume) is collected on a substrate placed a short distance from the target. Though the actual physical processes of material removal are quite complex, we can consider the ejection of material to occur due to rapid explosion of the target surface with superheating. Unlike thermal evaporation, which produces a vapor composition dependent on the vapor pressures of elements in the target material, the laser-induced expulsion produces a plume of material with stoichiometry close to the target. It is generally easier to obtain the desired film stoichiometry for multi-element materials using PLD than with other deposition technologies.

Some major advantages of pulsed laser deposition include:

1. It is the top choice for epitaxial deposition of oxide films.

2. It is conceptually simple. A laser beam ejects molecules from a target surface and produces a film on the substrate with the same composition as the target.

3. It is versatile. Many types of materials can be deposited.

4. It is cost-effective. One laser can serve many vacuum systems, with quality comparable to molecular beam epitaxy systems which cost 10 times more.

5. It is fast. High quality samples can be grown reliably in minutes.

6. It is potentially scalable. Complex oxide preparation can be achieved for industrial scale volume production.

Table 2.1 Comparison of major deposition methods

	PLD	Sputtering	MBE
Major Usage	oxide thin film epitaxial deposition	Metal film deposition	All material
Cost	Decent	Decent	High
Industry usage	Yes	Yes	only III-V and II-VI materials
Versatility	Yes	Somewhat	Yes
Speed	Relatively fast	Relatively fast	Slow

A variety of thin film deposition techniques have been employed for the preparation of oxide films similar to what are presented in this dissertation. Of all the techniques, PLD and MBE have yielded the best quality epitaxial films.

We use PLD as our primary sample preparation method. Some of the important factors determining the quality of the PLD deposited oxide thin films are the speed of growth, the

intensity of the laser power, photon frequency, ambient pressure, the choice of substrate, substrate temperature, and post-deposition annealing.

2.2 Deposition Principles and Deposition System

Thin film formation during PLD generally can be divided into the following four stages:

1. Laser radiation interaction with the target,
2. Formation of ablation plume,
3. Deposition of the ablated materials onto the selected substrate,
4. Nucleation and growth of thin film.

At Stage 1, high power pulsed laser beam ejects material from a small amount of area of the solid pellet target inside a high vacuum chamber. The absorbed energy is sufficient to break any chemical bonds of the molecules of target material, which are subsequently deposited as a thin film on a substrate. Usually, lasers with shorter wavelength (UV region) are preferred because at shorter wavelengths the energy of the photons are higher and the ablation occurs more efficiently. The fluence of a laser pulse [laser intensity, [J/cm^2]] has to be larger than a threshold value so that all the species can be stoichiometrically removed from the target.

At stage 2 - 4, the particle cloud absorbs a large amount of energy from the laser beam producing an expansion of hot plasma (plume) in the deposition chamber. The ablated species condense on the substrate placed opposite to the target, forming a thin film after some hundreds or thousands of laser pulses.

The schematics of a typical set up of a PLD system is shown in Fig. 2.1. It includes the laser system, deposition systems, and vacuum system which will be further discussed in sections 2.2.1, 2.2.2 and 2.2.3, respectively.

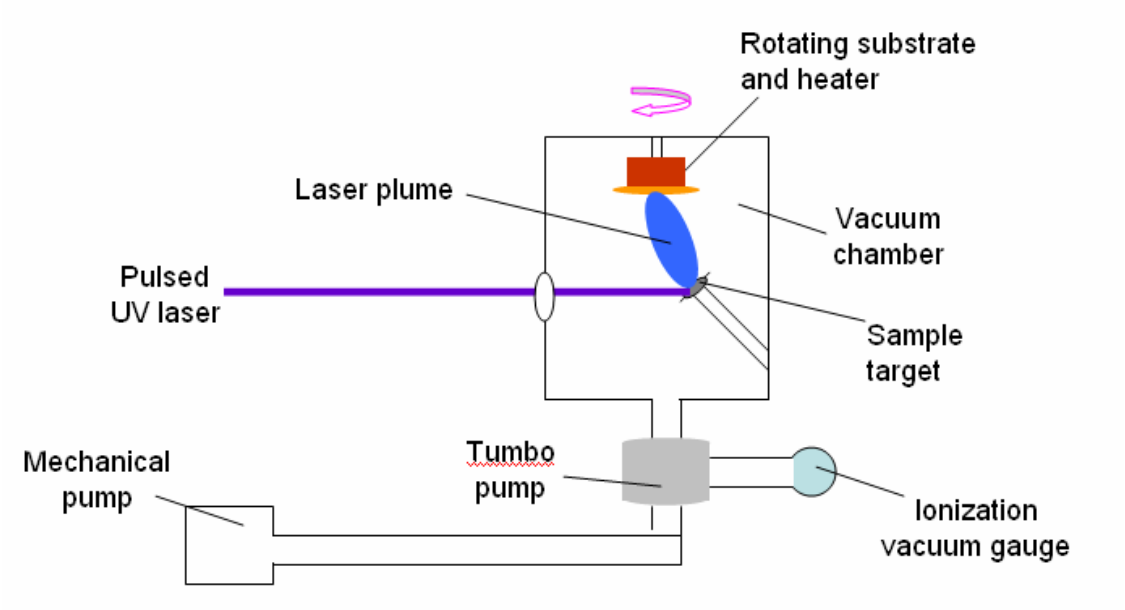

Fig.2.1 Basic set up for Pulsed Laser Depostion

2.2.1 Lasers

2.2.1.1 Laser Sources -- Solid state Lasers and Excimer Lasers

In general, the useful range of laser wavelengths for thin-film growth by PLD lies between 200 nm and 400 nm. Most target materials used for deposition exhibit strong absorption in this spectral region. Both excimer and Nd^{3+}:YAG laser are used as the laser source.

The excimer laser is a gas laser system; it emits radiation directly in the UV. These systems have high outputs delivery and achieve pulse repetition rates up to several hundreds Hertz with energies near 1 J/ pulse. Excimer KrF has the highest gain among systems with wavelength 248 nm.

Nd^{3+}:YAG lasers are solid state alternatives to excimers lasers that are increasingly being used in research laboratories. The neodymium ions serve as the active medium and are present as impurities in the YAG host. The neodymium ions are pumped optically into their upper states by flashlamps. High output energies are achieved by using two YAG rods in an oscillator/amplifier configuration. The fundamental laser emission of Nd^{3+}:YAG occurs at 1064 nm, which can be frequency doubled with about 50% power conversion efficiency yielding an output at 532 nm. With further doubling the frequency, the outputs at 355 nm or 266 nm are produced.

2.2.1.2 Laser-Target Interaction

The interaction between laser pulses and the target depends strongly on the intensity of the incoming laser beam in addition to wavelength. In PLD, the intensity is typically brought to the order of 10^8-10^9 W/cm^2 by a focusing lens. The pulse duration is of a few nanoseconds.

The mechanisms energy transferred to the target can be understood as follows: The photon energy is initially absorbed by ionization and electronic excitation. After a few picoseconds, the energy is transferred to the crystal lattice, and during the laser pulse, within a few nanoseconds, a thermal equilibrium between the electrons and the lattice is reached. This leads to a strong heating of the lattice and, with continued irradiation, to a massive particle emission from the surface.

2.2.2 Deposition Systems

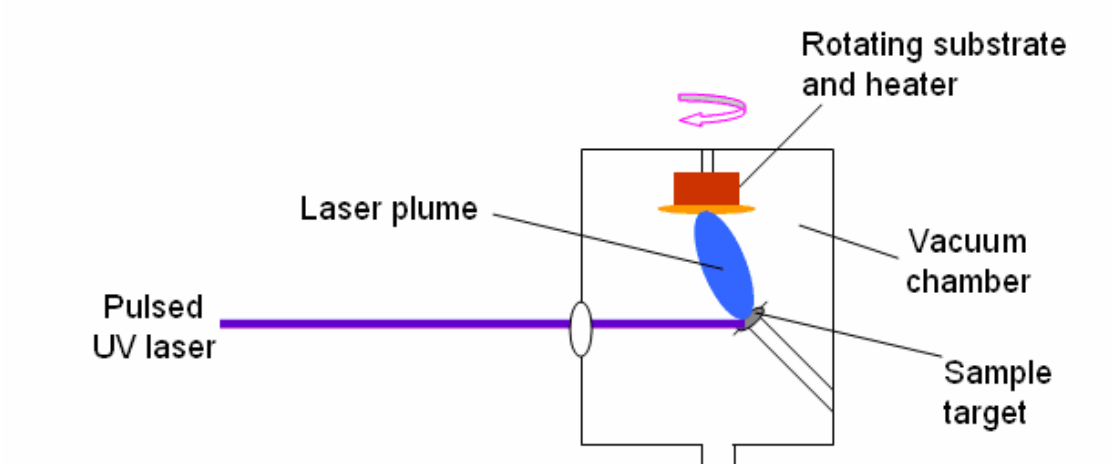

Fig. 2.2 Sketch of a PLD deposition chamber

The temperature of deposition also needs to be selected appropriately. In our experiment, for epitaxial growth of rutile structure thin films, the substrates were heated 700 °C. Some target materials are quite sensitive to a change in the deposition temperature; a decrease of only a few degrees from the optimal value may significantly degrade the crystal quality and the properties of

the film. A lower temperature also increases the formation of particulates and lattice defects. In our experiment, the thin films become amorphous structure if grown at temperature 300 °C.

To obtain epitaxial growth, the lattice structures of the substrate and expected thin film need to be match with each other. The uniformity and crystallinity of the film can be further increased by rotating the target (360° endless) during the deposition process (so that laser pulses will not strike all the time the same spot on the target surface).

The oxygen pressure inside the chamber can be adjusted in order to accommodate growing of different oxide films. The laser-pulse repetition rate is adjusted so that it is low enough for the ablated species to have time to form a smooth layer between successive pulses. Too low a repetition rate has to be avoided since fast chemical reactions may hinder the epitaxial growth of the film. Pulse duration of the laser, repetition rate and spot size on the target also need to be optimized in order to minimize the number of particulates that come out of the target surface when collecting too much of energy in a single pulse.

2.2.2.1 Ablation Plume

Some atoms in the vapour from the ejected material are ionized. The particle cloud absorbs energy from the laser beam and becomes more ionized. Finally, fully ionized plasma is formed in the vicinity (about 50 μm) of the target[16]. The plasma expands away from the target, with a strongly forward-directed supersonic velocity distribution. A photograph of the plume is shown in Fig. 2.3. The visible part of the particle jet is referred to as an ablation plume. The plume consists of several types of particles: neutral atoms, electrons, and ions. Furthermore, clusters of different compounds of the target elements are observed near the target surface. The visible light of the plume is due to fluorescence and recombination processes in the plasma.

Fig. 2.3 Photograph of the plume[17]

2.2.3 High Vacuum System

High vacuum (HV) is the regime characterized by pressure from 1×10^{-3} to 1×10^{-9} Torr (100 mPa to 0.1 μPa). HV requires the use of special materials, cleanliness, and baking the entire system to remove water and other trace elements. Pressure is measured by an ionization vacuum gauge. At low pressure, gas molecules rarely collide. The mean free path of a gas molecule at 10-5 Pa (~10−7 Torr) is approximately 40 km, so gas molecules will collide with the chamber walls many times before colliding with each other. Almost all interactions therefore take place at various surfaces in the chamber.

HV is necessary for our thin film growth to reduce surface contamination, by reducing the number of molecules reaching the sample over a given time period. At 0.1 mPa (10^{-6} Torr), it only takes 1 second to cover a surface with a contaminant, so relatively lower pressures are needed for long experiments to minimize the contamination of the films.

To achieve HV, a system needs the following:

- High pump speed
- Minimized surface area in the chamber
- High conductance tubing to pumps — short and fat, without obstruction
- Use low-outgassing materials such as certain stainless steels
- Avoid creating pits of trapped gas behind bolts, welding voids, etc.
- Electropolish all metal parts after machining or welding
- Use low vapor pressure materials (ceramics, glass, metals, teflon if unbaked)
- Bake the system (250 °C to 400 °C) to remove water or hydrocarbons adsorbed to the walls
- Chill chamber walls to cryogenic temperatures during use
- Avoid all traces of hydrocarbons, including skin oils in a fingerprint — always use gloves

In our setup, base vacuum pressure during deposition better than 10^{-7} Torr is ensured by the Turbo V-550 turbo molecular pump (Varian Vacuum Products), which is supported by a mechanical fore-pump. Deposition can be made in vacuum or in the presence of reactive gases with pressures up to a few mTorr.

2.3 Film Growth by Pulsed Laser Deposition.

2.3.1 Substrate Materials for O-DMS Films

High-temperature O-DMS films have been grown successfully on many different substrates. A general requirement for a good substrate material is that, for certain orientations, the lattices of the substrate and film match. Thermal expansion coefficients of the materials should also be close such that the film does not break during the cool down to low temperatures. If the mismatch of either of these parameters is large, the maximum thickness of the film that can be grown epitaxially, if at all, is limited. Furthermore, a proper substrate material does not react chemically with the film and preferably is compatible with semiconductor technology. In addition, device applications impose a number of additional requirements on the substrate. Depositing films on these substrates is a rather straightforward process and, therefore, they are used in the preparation of several microelectronic components. On the other hand, the films often have a large dielectric constant, which should be taken into consideration.

Substrates we use include *R*-plane α-Al_2O_3 (012) for SnO_2 film deposition and Si (400), Al_2O_3 (012) and $LaAlO_3$ (100) for HfO_2 film deposition

2.4 Thin Film Characterization

2.4.1 X-Ray Diffraction

X-ray diffraction (XRD) is one of the most important non-destructive tools to analyse all kinds of materials - ranging from films to powders and crystals. From research to engineering and production, XRD is an important tool for materials characterization and quality control. In our research, we use a Philips X'pert PW3040 MPD diffractometer using Cu Kα to identify the specimens' crystal structure and crystallographic orientation of the films.

2.4.2 Physical Properties Measurement System (PPMS)

Physical properties measurement system (PPMS) manufactured by Quantum Design was used to make most of the electron transport measurements. The specific equipment used was Model 6000 PPMS. This model allows for variable temperature and magnetic field measurements. The temperature range is from 1.9 K to 400 K, and the magnetic field can go up to 14 T. The cooling of the PPMS and the superconducting magnet inside is via liquid helium introduced into a region called cooling annulus (shown in figure 2.5).

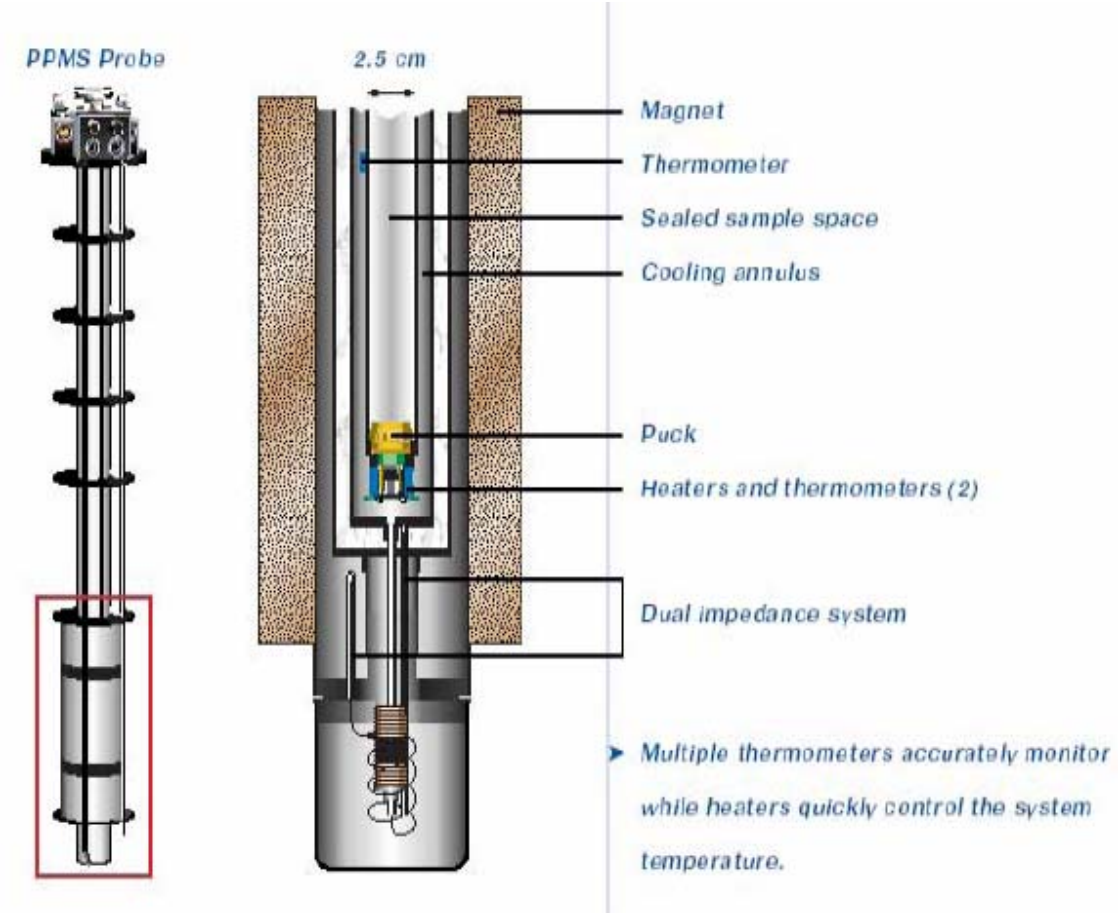

Figure 2.5: Cutout diagram of PPMS 6000 by Quantum Design [Copyright Quantum Design].

2.4.3 Superconducting Quantum Interference Device (SQUID)

Fig.2.6 SQUID equipment (MPMS XL-7T, Quantum Design, Inc)

SQUID utilizes the superconducting quantum interference effect and can make the most sensitive magnetic measurements to date. The MPMS-XL7 from Quantum Design, Inc (Fig. 2.6) is capable of changing the magnetic field between -7 to 7 Tesla. The measurements can be carried out at any temperature with accurate temperature control from 1.9 to 400 K. The differential sensitivity is 10^{-8} emu and the instrument can make both DC & AC susceptibility measurements.

The four-point-probe method was used to measure the electrical transport properties of the thin films. Fig. 2.7 shows a schematic diagram of the four-point-probe measurement set-up. In the figure shown, the current is applied through probes 1 and 4 and the voltages measured between probes 2 and 3[18].

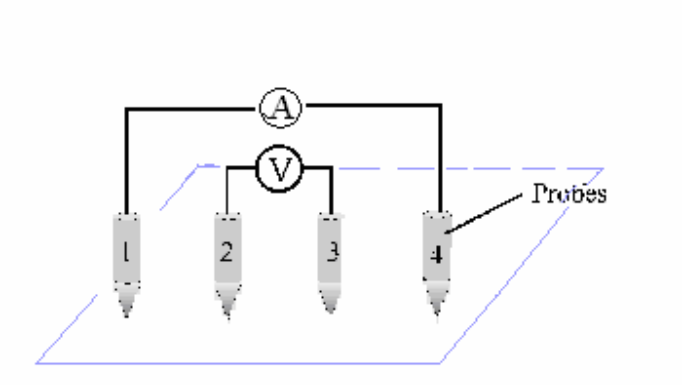

Figure 2.7: Schematic of a four-point-probe measurement set-up for a thin film

2.4.4 Transmission Electron Microscope (TEM)

Transmission electron microscope (TEM) operates on the same basic principles as the light microscope but uses electrons instead of light. Therefore TEM is limited by the wavelength of the electrons. TEMs use electrons as the "light source" and their much lower wavelength makes it possible to get a resolution a thousand times better than with a light microscope. We can see objects at a scale of a few angstroms.

A "light source" at the top of the microscope emits the electrons that travel through vacuum in the column of the microscope. Instead of glass lenses focusing the light in the light microscope, the TEM uses electromagnetic lenses to focus the electrons into a very thin beam. The electron beam then travels through the specimen one wants to study. Depending on the density of the material present, some of the electrons are scattered and disappear from the beam.

At the bottom of the microscope the unscattered electrons hit a fluorescent screen, which gives rise to a "shadow image" of the specimen with its different parts displayed in varied darkness according to their density. The image can be studied directly by the operator or photographed with a camera[19].

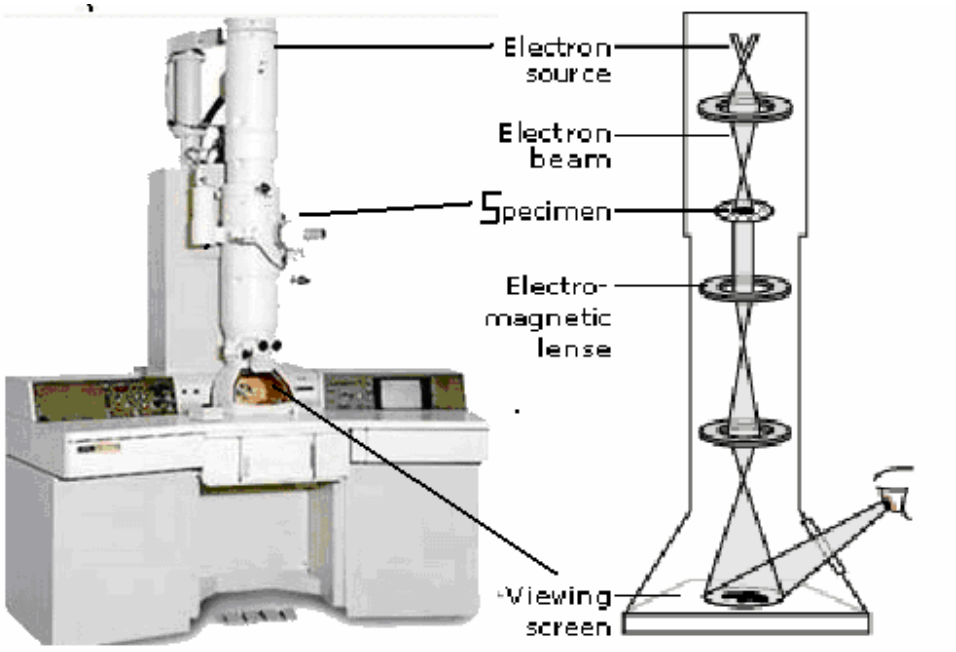

Fig. 2.9 Transmission Electron Microscope

The TEM we use is a JEOL 2010 Transmission Electron Microscope, which has a wide range of capabilities such as high-resolution image observation with 0.23 nm point resolution and 0.14 lattice image, EDS (Energy dispersive X-ray spectrometry) for element analysis, and versatile analysis by electron diffraction. The magnification goes from 1,500 to 1,200,000×. The Maximum accelerating voltage is 200kV.

CHAPTER 3

THE STRUCTURE AND MAGNETIC PROPERTIES OF TIN DIOXIDE THIN FILMS

3.1 Introduction

In the studies of room-temperature ferromagnetism (RTFM), there are various types of transition-metal (TM) doped-oxide thin films, such as TM-doped ZnO, TM-doped TiO_2, or TM-doped SnO_2. There are a number of controversial issues that need to be clarified[20]: for example, why a clear correlation between the Curie temperature T_C and the concentration of the magnetic dopant element has not been established; and why doping by nonmagnetic elements, such as V and Cu[21], can sometimes result in strongly ferromagnetic samples; why, in some cases, bulk samples are not magnetic but the thin films of the same compositions are magnetic. In these materials, the ferromagnetism cannot simply be attributed to a secondary phase, although existing theories of magnetism can not explain it. Several mechanisms are possible: carrier mediated exchange coupling, spin polarons, short range superexchange, and defects induced magnetism. Furthermore, in DMS, nonmagnetic host ions are partially substituted by the magnetic dopants, which are randomly localized over the host lattice. Thus, it is difficult to use a simple theory to completely explain everything.

Following the initial discovery of room temperature ferromagnetism in Co-doped TiO_2 of anatase structure, ferromagnetism was also found in doped TiO_2 rutile thin films. The latter seems more interesting from many perspectives. For example, the anomalous Hall Effect[22], a key indication of a genuine ferromagnetic state, and magnetic circular dichroism[23] has been

simultaneously observed in rutile films that exhibit ferromagnetism[24]. Researchers are thus looking at other materials having the same rutile-type structure.

SnO_2 a wide band gap semiconductor with E_g=3.6 eV[25], and up to 97% optical transparency in the visible range, crystallizes in rutile structure, Measurements of magnetic properties of TM doped SnO_2 vary vastly. Mn-doped SnO_2 was reported to show a large magnetoresistance at low temperature and paramagnetic behaviour[26]. While others reported that it is ferromagnetic with T_C equal to 340 K[27]. Fe and Co-doped SnO_2 have been found to be ferromagnetic with T_C ranging from 360 K to 650 K.[28, 29, 30] Co-doped films have a rather high magnetization of 7.5μ_B per Co and 7.5μ_B per Co respectively.[31,32] Ni-doped SnO_2 was reported to have a T_C = 400 K and magnetization of 2μ_B per Ni.[33, 34, 35] Some synthesized powder[36] such as $Sn_{0.99}Fe_{0.01}O_2$ also showed high Curie temperature T_C=850 K. Much of these results are still controversial due to the difficulty in resolving the true origin of the observed magnetic signals. In order to clarify the confusion about these experimental results and for the reasons given above, we have investigated Cr and Fe doped SnO_2 films grown by PLD and studied their magnetic and transport properties.

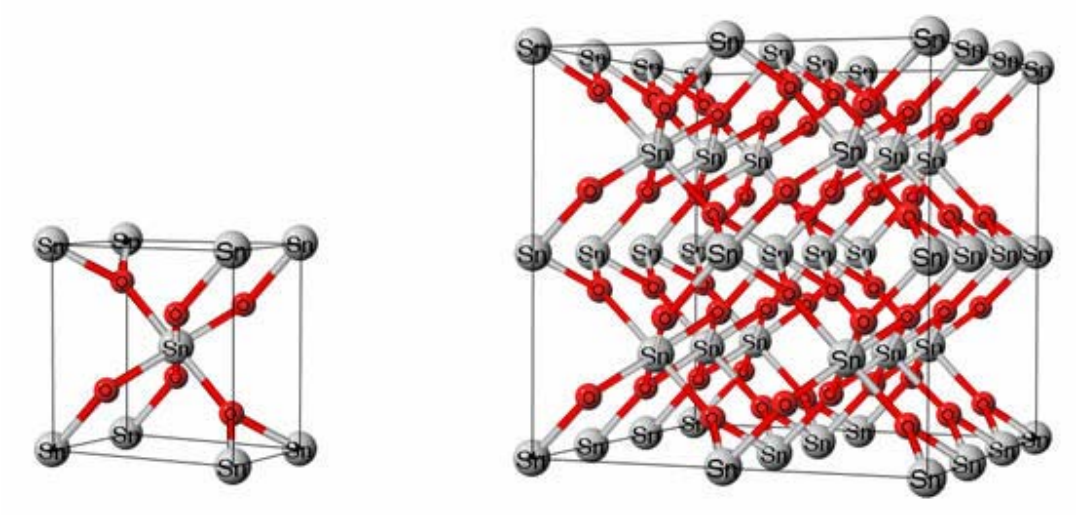

Fig. 3.1 Rutile structure SnO_2[37]

3.2 Experiments

$Fe_xSn_{1-x}O_2$ and $Cr_xSn_{1-x}O_2$ (x = 0, 0.02, 0.06, 0.10, 0.20) thin films were grown on α-Al_2O_3 (012) substrates by PLD. Before deposition, the substrates were put in strong acid (HCL : HNO_3 ~ 3: 1) for 20 hours, to remove the weak ferromagnetic signal (about 10^{-5} emu) found in the as-purchased substrates. The targets were prepared using standard ceramic techniques. The films were prepared in vacuum at a substrate temperature of 970 K. The pressure during deposition was 2×10^{-6} Torr. The pulsed excimer laser uses KrF (λ= 248 nm) and produces a laser beam of intensity (fluence) of 1–2 J/cm^2 and repetition rate of 10 Hz. The Fe concentration of the films was measured with energy dispersive x-ray analysis in TE mode, and was consistent with those of the targets. The crystal structure was investigated by x-ray diffraction (XRD) with Cu K$_\alpha$ radiation. The magnetic properties were studied with a superconducting quantum

interference device (SQUID) magnetometer. The transport properties were measured with a physical property measurement system (PPMS) from Quantum Design.

3.3 Results and Discussion

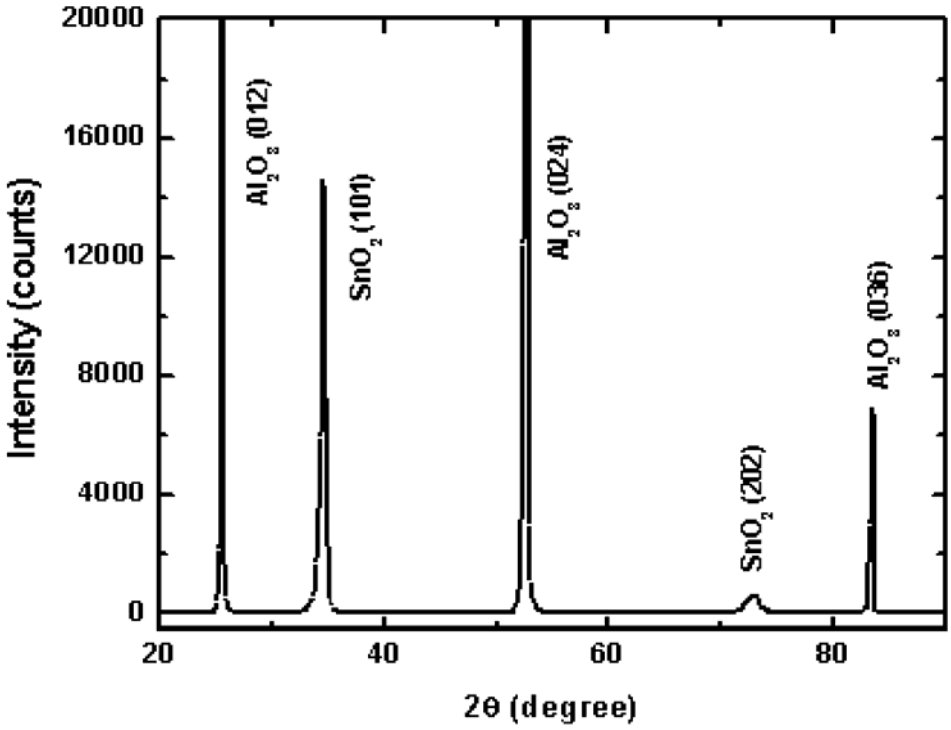

Fig. 3.3 XRD diffraction pattern of Cr0.2Sn0.8O2 film.

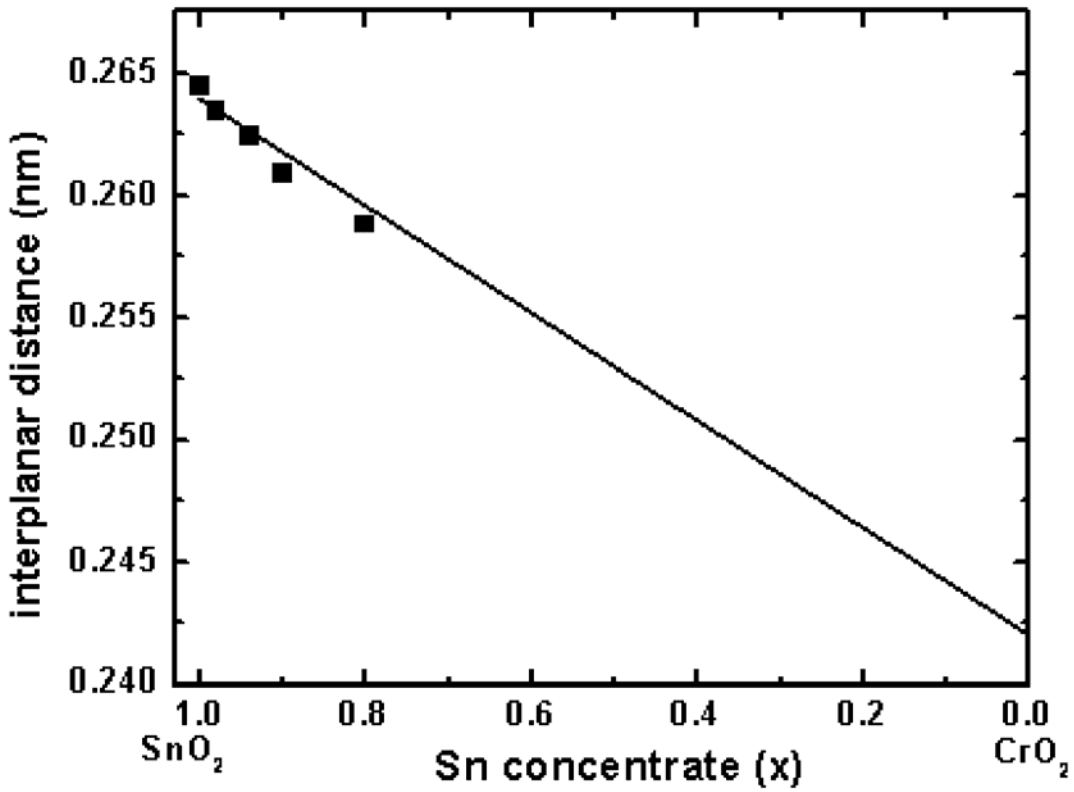

Fig.3. 4 Interplanar spacing of (101) plane as a function of Cr concentration.

Solid line is the theoretical value and dots are our experimental results.

Figure 3.3 shows the XRD pattern for a $Cr_{0.2}Sn_{0.8}O_2$ film grown on *R*-plane α-Al_2O_3 (012). The film is single phase and of rutile type with (101) plane parallel to the film plane. The two peaks show (101) and (202) reflections of doped SnO_2. The other three peaks are from the substrate α-Al_2O_3 (012), (024) and (036). Similar XRD patterns were obtained for all films with different Cr and Fe contents suggesting that the films are epitaxially grown. These results are

consistent with the work of other groups.[11, 10] For Fe-doped SnO_2 films with fast deposition rate, XRD patterns reveal impurity phases in the films.

Detailed study of SnO_2 (101) and (202) peaks of $Cr_xSn_{1-x}O_2$ thin films reveals that they have a systematic shift toward higher angles, which means that the interplane spacing decreases continuously with the increase of Cr concentration (See Figure 3.4). CrO_2 also crystallizes in rutile structure. If we assume that Cr substitutes Sn continuously in SnO_2, the interplanar spacing should exhibit a linear change with Cr concentration as is indeed shown in Figure 2. This clearly indicates that Cr dissolves in SnO_2. On the other hand, for Fe doped SnO_2 film, the interplanar distance is almost independent of the Fe concentration, up to 20% doping. Since the radius of Sn (IV) ion is 0.083 nm whereas the radii of Fe (III) and Fe (IV) ions are 0.069 and 0.0725 nm, respectively, doping Fe in SnO_2 should have resulted in a change of lattice parameter of SnO_2. Our XRD result does not indicate that Fe dissolves in SnO_2.

The observation of room-temperature ferromagnetism in these materials must be accompanied by a careful identification of the phases and microstructures present in order to accurately identify the origin of the magnetism[11,38] as will be discussed in detail in next chapter.

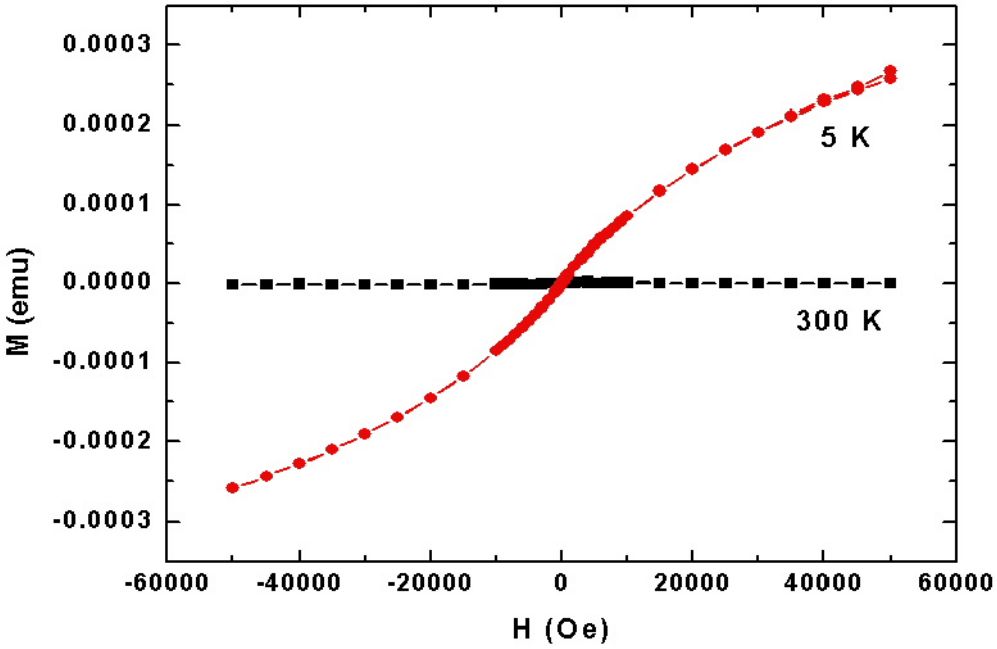

Fig. 3.5 Magnetization curves of $Cr_{0.2}Sn_{0.8}O_2$ film measured at 5 K and room temperature. The magnetic field was applied parallel to the film surface.

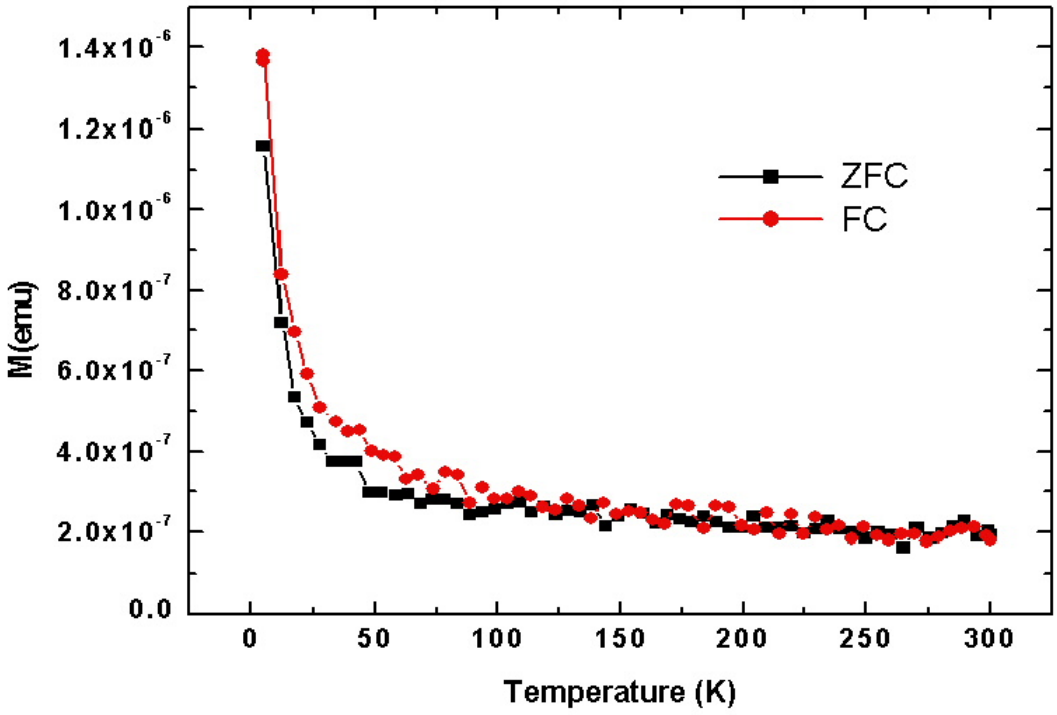

Fig. 3.6 $Cr_{0.2}Sn_{0.8}O_2$ ZFC-FC curves with H = 100 Oe.

Magnetic properties of Cr doped SnO_2 films are shown in Fig. 3.5. The hysteresis loops show that all Cr-doped films are paramagnetic at 300 and 5K, which is different from a recent report.[11] A very weak ferromagnetic signal of about 1×10^{-6} emu was observed in all Cr-doped samples. Since this kind of signal also appears in pure SnO_2 samples, we do not think it comes from doped Cr. Both ZFC and FC curves (see Fig. 3.6) show a temperature dependence of magnetic susceptibility that fits Curie-Weiss law, which is another evidence of paramagnetism in Cr doped SnO_2 samples.

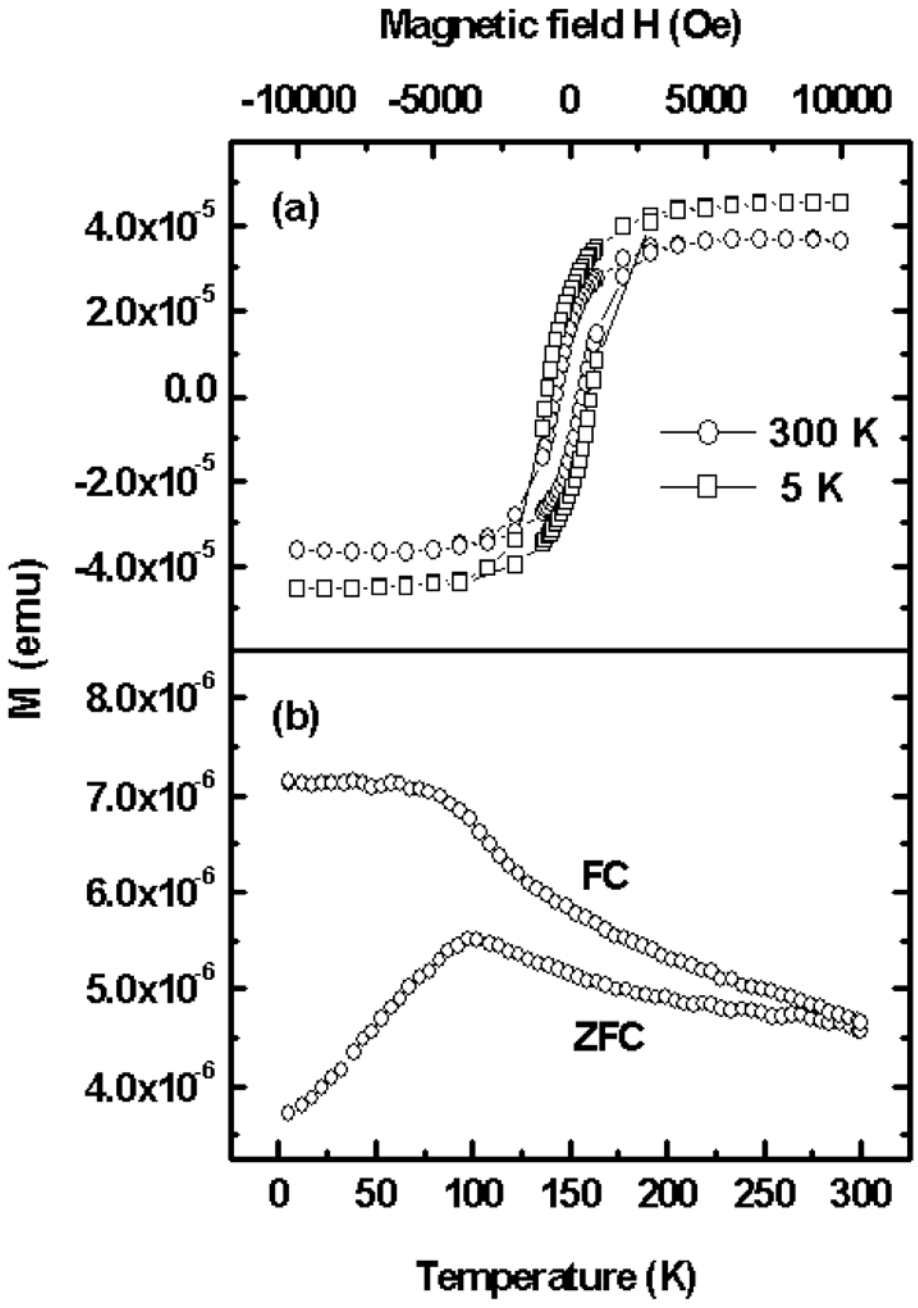

Fig. 3.7 Temperature dependence of resistance for $Fe_{0.06}Sn_{0.94}O_2$ film.

Magnetic properties of Fe doped SnO_2 films are shown in Figure 3.7. The hysteresis loop exhibits ferromagnetic property at room temperature as reported previously. The coercivity of the films is about 500 Oersted. At 5 K, the hysteresis loop exhibits similar behavior to the ones at room temperature except that the coercivity increases to about 800 Oersted and magnetization increases slightly. The magnetic moment per Fe atom is 1.0 μ_B/Fe. ZFC-FC curves exhibit a blocking temperature of about 100 K. This blocking behavior implies that there are precipitated ferromagnetic particles in the films which are partially responsible for the ferromagnetic property of Fe-doped SnO_2. The hysteresis observed at room temperature indicates that some larger particles are not yet superparamagnetic and are still blocked.

The transport measurements indicate that the Fe doped SnO_2 films have very high resistance (about 10^7 ohm) at room temperature and the temperature dependence of the resistance is characteristic of a semiconductor with an activation energy of about 230 meV (Figure 3.8). The activation energy is sensitive to the oxygen pressure during the preparation, varying from tens of meV (in vacuum) to hundreds of meV (in air) for pure SnO_2, [39] and is also depend on the doping elements and doping level. Coey *et al.* reported an activation energy of 75 meV in Fe doped SnO_2 after heating in vacuum[12]. It is not clear whether the observed value of 230 meV is associated with the presence of Fe or the amount of oxygen vacancies. Neither magnetoresistance signal nor anisotropic magnetoresistance (AMR) effect has been observed. The observation of the latter would be an indication of intrinsic ferromagnetism.

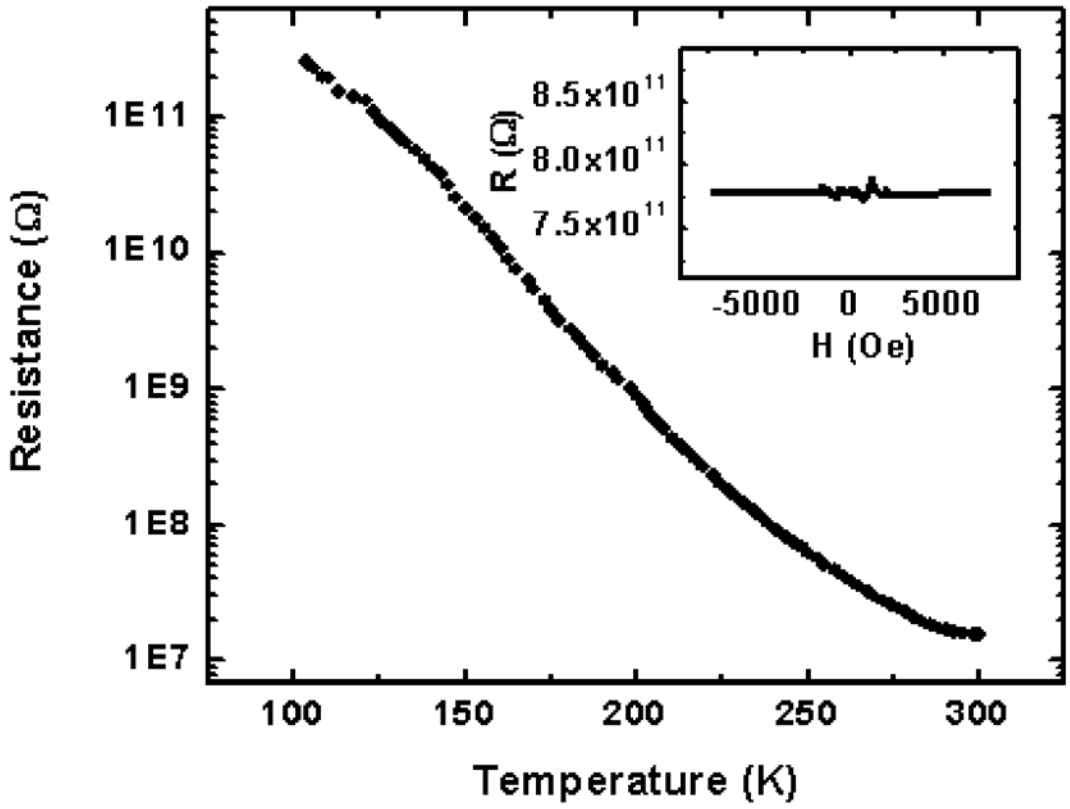

Fig. 3.8 Temperature dependence of resistance for Fe doped SnO_2 film

3.4 Conclusions

We have prepared Cr and Fe-doped SnO_2 films by PLD. X-ray diffraction patterns show that the films are of rutile structure and grown along (101) plane. The diffraction peaks of Cr-doped SnO_2 exhibit a steady shift toward higher angles with increasing Cr concentration. This indicates that Cr dissolves in SnO_2. On the other hand, XRD experiments do not show similar results for Fe-doped films. The magnetization curves indicate that the Cr-doped SnO_2 films are

completely paramagnetic. The Fe-doped SnO_2 samples are ferromagnetic at 300 and 5 K. Zero-field-cooled (ZFC) and field-cooled (FC) curves indicate there are ferromagnetic particles in the films which behave superparamagnetically above the blocking temperature of about 100 K. The anisotropic magnetoresistance effect was not observed in the Fe doped SnO_2 samples.

CHAPTER 4

ROLE OF DEFECTS IN TUNING FERROMAGNETISM IN DILUTED MAGNETIC OXIDE THIN FILMS

4.1 Introduction

As discussed in chapter 3, we have synthesized the Cr and Fe doped SnO_2 films which were deposited on Al_2O_3 substrates by pulsed laser deposition. X-ray diffraction patterns show that the films have rutile structure and grown epitaxially along (101) plane. The transport measurements indicate that the Fe doped SnO_2 thin films show high resistance (about 10^7 ohm) at room temperature and the temperature dependence of the resistance is characteristic of a semiconductor with calculated activation energy of about 230 meV. It is known that the activation energy depends sensitively on the oxygen pressure during the preparation and varies from tens of meV (in vacuum) to hundreds of meV (in air) for pure SnO_2.[40] It also depends on the doping elements and doping level. Coey *et al* [41] reported an activation energy of 75 meV in Fe doped SnO_2 after heating in vacuum. Since we have not done a systematic study on the oxygen content and Fe doping dependence of the activation energy, it is difficult to speculate whether the observed value of 230 meV is associated with the presence of Fe. However, the difference between the values of this study and Ref. 41 may suggest that our samples contain less oxygen vacancies than the heat treated sample.

As mentioned in Chapter 3, the origin of the ferromagnetism at room temperature is still an open question. Our previous study on Fe-doped TiO_2 and other investigations suggest that oxygen deficiency is important for the samples to exhibit ferromagnetism [2]. Oxygen vacancies were proposed as the origin for the ferromagnetism observed in undoped HfO_2.[42] Various experiments and theoretical models suggest that oxygen vacancy may play a critical role in the magnetism[43,44],[1]. We continue this investigation and try to understand the relationship of oxygen vacancy with respect to the magnetic properties in Cr doped SnO_2 thin films.

4.2 Experiment

$Cr_xSn_{1-x}O_2$(x = 0, 0.02, 0.06, 0.10, 0.20) thin films were grown on α-Al_2O_3 (012) substrates in vacuum at a substrate temperature of 970 K by PLD technique (KrF, λ= 248 nm, 1–2 J/cm^2 10 Hz.). Before deposition, the substrates were put in a strong acid (HCl: HNO_3 ~ 3: 1) for 20 hours.

In order to elucidate the effects of oxygen vacancies on magnetism, selected samples of Cr:SnO_2 were also postannealed at 300 °C, 400°C, 500°C, 600°C during 10-12 hours in flowing H_2 atmosphere..

The Cr concentration of the films was measured with energy dispersive x-ray analysis in TE mode, and they were consistent with those of the targets. The crystal structure was investigated by x-ray diffraction (XRD) with Cu K_α radiation. The magnetic properties were studied with a superconducting quantum interference device (SQUID) magnetometer. The transport properties were measured with a physical property measurement system (PPMS) from Quantum Design. The magnetic properties were measured by a superconducting quantum

interference device (SQUID) system from 5 K to 300K. For both magnetism and magnetoresistance measurements, the magnetic field is applied in the film plane. Although the samples with various $Sn_{1-x}Cr_xO_2$ compositions were prepared, here we mainly report the experimental results of the $Sn_{0.98}Cr_{0.02}O_2$ sample.

4.3 Experimental Results and Didcussion

4.3.1 SEM result

The microstructures of the samples were examined using scanning electron microscopy (SEM). It is observed that heat treatment at different temperature of ambient have noticeably different effects on the thin film. For annealing temperatures of 400°C and above, the thin films were destroyed, as shown in the SEM photos in Fig. 4.1. At annealing temperatures below 300°C, the crystal structure of the films were still retained while the resistivity decreases.

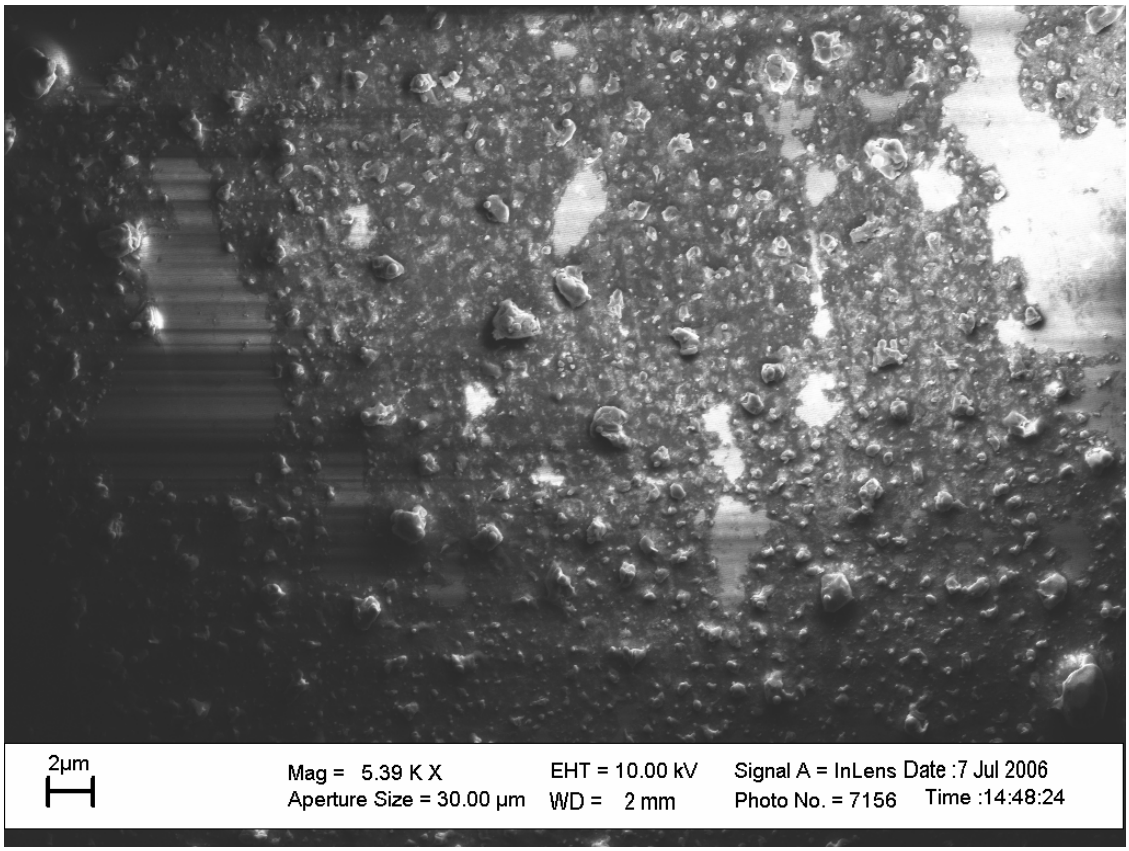

Fig.4.1 SEM photos of $Cr_{0.02}Sn_{0.98}O_2$annealed at temperatures of 600°C.

4.3.2 Magnetic properties

Figure 4.2 shows the comparison of the hysteresis loops measured at 5 K and 300 K, after and before the H_2 treatment. The M[H] curves show a well defined hysteresis loop, note that the shape of M[H] curves taken at 300 and 5K are quite similar indicating that the samples are certainly in a ferromagnetic state over a certain range of temperature. The ferromagnetism is clearly shown by the coercivity, remanence, and the low saturation field after H_2 treatment in both 5 K and 300 K. The data leads us to conclude that annealing in hydrogen leads to a ferromagnetic state in Cr-doped SnO_2 at room temperature. As for the origin of the

ferromagnetism, it may be attributed to the oxygen vacancies induced by the H_2. The defect levels created by the O vacancies can supply s, p carriers and lead to the spin-spin exchange interaction between the s, p carriers and the localized d electrons of Cr. There may be also direct d-d exchanges interaction between the neighbor Cr atoms if Cr atoms segregate in the host lattice, however this latter scenario is less likely in our samples.

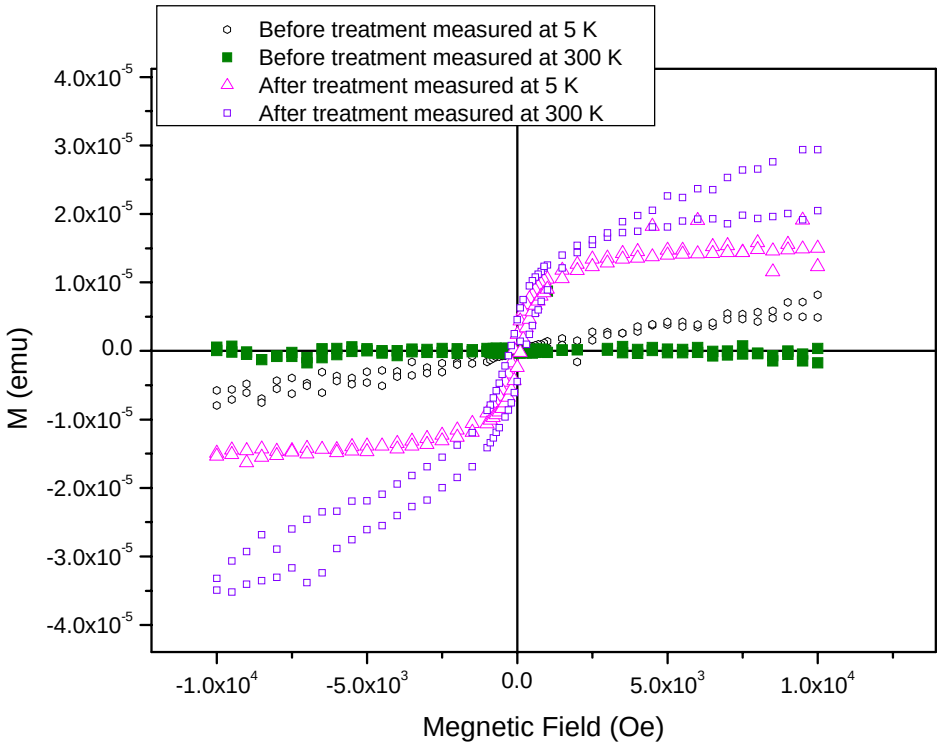

Figure 4.2 The comparison of hysteresis loops measured at 5K and 300 K, after and before the H_2 treatment respectively

4.3.3 Resistance vs Temperature

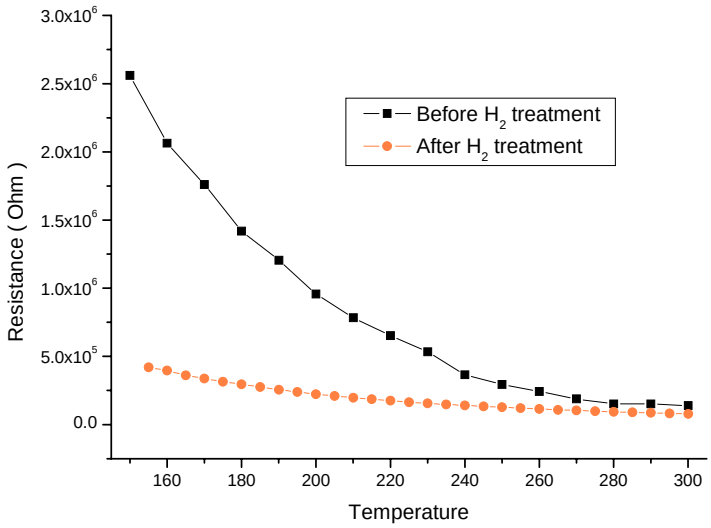

Fig. 4.3 Resistance vs Temperature of 2% Cr doped thin film before and after H_2 treatment under 300°C

The film has the resistivity in the range of semiconductor and shows semiconducting temperature dependence in Fig. 4.3 and the magnetic moment increase after the H_2 treatment. Fig. 4.4 indicates that the activation energy of the Cr-doped SnO_2 films dropped from 81.506 meV to 47.076 meV when using $\ln R = \ln R_0 + \frac{E_a}{k}\frac{1}{T}$ within temperature range from 160K to 300K. Therefore, we conclude that the annealing in a reducing atmosphere does decrease the activation energy as a result of increased oxygen vacancies in the films, and changes the magnetic properties of the film. The thin films did not show any AMR.

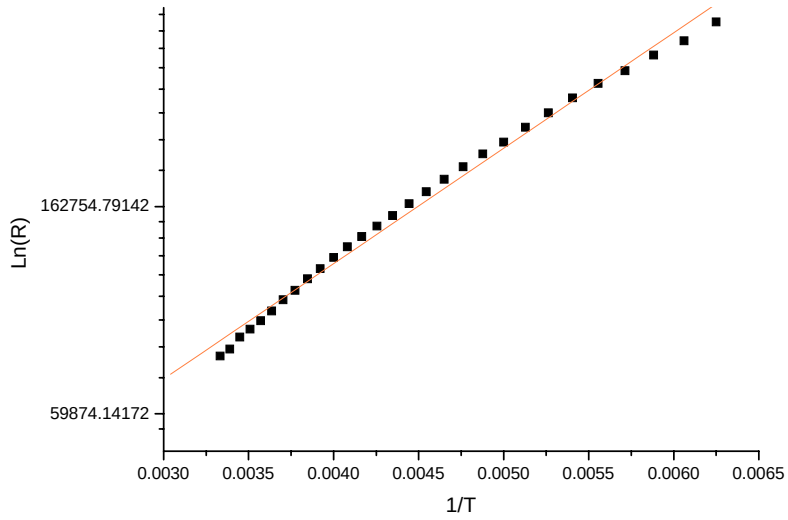

Fig. 4.4 Linear fit for Cr-doped SnO_2 thin film before H_2 treatment at higher temperature from 160K to 300K Label axes

4.4 Conclusions

In summary, $Sn_{0.98}Cr_{0.02}O_2$ magnetic semiconductors were synthesized. Composition analysis and XRD patterns indicated that Cr element was incorporated into SnO_2. The film obtained after H_2 treatment is ferromagnetic at room temperature as confirmed by the magnetic hysteresis curves shown in Fig. 4.2, it is also confirmed by the ZFC-FC results. From our transport measurement, we calculated the activation energy, which did decrease from 81.506 meV to 47.076 meV, which can be explained by the increase in the defects/oxygen vacancies by H_2 treatment of the films. In this system, local Cr atoms may establish long range ferromagnetic ordering through sp-d interaction and local ferromagnetic ordering through direct d-d exchange

interaction between the neighbouring Cr atoms. The anisotropic magnetoresistance (AMR) was not observed in the samples.

We also attempted to repeat the similar H_2 treatment in our 6% Cr doped thin film sample, but did not obtain confirming results because of the phase change of the film.

CHAPTER 5

STRUCTURE AND MAGNETIC PROPERTIES OF PURE AND GADOLINIUM-DOPED HAFINIUM DIOXIDE THIN FILMS

5.1 Introduction

HfO_2[45], CaB_6[46,47,48,49] and CaO[50] have been found, or predicted, to exhibit unusual ferromagnetic behaviors, which can not be explained by the conventional mechanisms for ferromagnetism (ferromagnetism contributed by magnetic ions). Theoretical calculations indicate their ferromagnetism may be related to cation or anion vacancies. It has been proposed[51, 52] that thin film deposition processes may create necessary oxygen vacancies to provide carriers and induce magnetic moments, which establish magnetic states. Such hypothesis is currently being debated and demands experimental study.

HfO_2 is a wide-band insulator with high dielectric constant. The possibility of making the material ferromagnetic may widen their applications in spintronics. As nonmagnetic as HfO_2 is, the discovery of ferromagnetic phenomenon in pure thin films[53] was a surprise. These films are found ferromagnetic, with a Curie temperature exceeding 500 K and a magnetic moment of about 0.15 Bohr magnetons per HfO_2 formula unit. The magnetization of the thin films is remarkably

anisotropic, being up to three times greater when the magnetic field is applied perpendicularly to the plane of the film than when it is applied in the parallel direction.

Since dielectric oxide HfO_2 films, where neither Hf^{4+} nor O^{2-} is magnetic, may leave Hf atoms with an empty *d* shell, the phenomenon was initially termed d_0 magnetism. It was suggested that the magnetism probably arose from partially filled *d* orbitals originating from hafnium atoms coordinating oxygen vacancies (*V*O). The isolated cation vacancies in HfO_2 could form high-spin defect states, and therefore, could be coupled ferromagnetically with a rather short-range magnetic interaction resulting in a ferromagnetic state

In this chapter, I report the synthesis of pure and Gd-doped HfO_2 powders and thin films and discuss their structure, transport and magnetic properties. The goal is to investigate the effects of defects, controlled through annealing, on the magnetic properties of both the thin films and powers.

5.2 Pure HfO_2 Thin Films

5.2.1 Experiments

Pure and Gd-doped HfO_2 targets were prepared by standard ceramic techniques using both 99.99% and 99.995% pure HfO_2 and 99.99% pure Gd_2O_3 powders. The thin films were deposited on single crystal silicon (400), *R*-Al_2O_3 (012), and $LaAlO_3$ (100) substrates using a KrF excimer laser with substrate temperature of 700±20 °C. The laser was operated at 10 Hz and was focused through a 30 cm focal length lens onto a rotating target at 45° angle of incidence. The energy density of the laser beam at the target surface was maintained at 1–2 J/cm^2. The target-to-

substrate distance was about 3 cm. Films were deposited with a base pressure of 5×10^{-7} Torr at a growth rate of about 0.15 Å/s.

The crystal structure of the films was investigated by x-ray diffraction (XRD) with Cu Kα radiation and high resolution transmission electron microscopy (HRTEM) with energy dispersive spectroscopy (EDS). The magnetic properties were studied with a superconducting quantum interference device (SQUID) magnetometer.

5.2.2 Structure Analysis

Figure 5.1 is the XRD pattern of a pure HfO_2 thin film deposited on Si (400) substrate. Besides Si substrate peaks, the rest peaks match the simple monoclinic phase of HfO_2. Similar XRD patterns have been obtained for HfO_2 films deposited on Al_2O_3 and $LaAlO_3$ substrates.

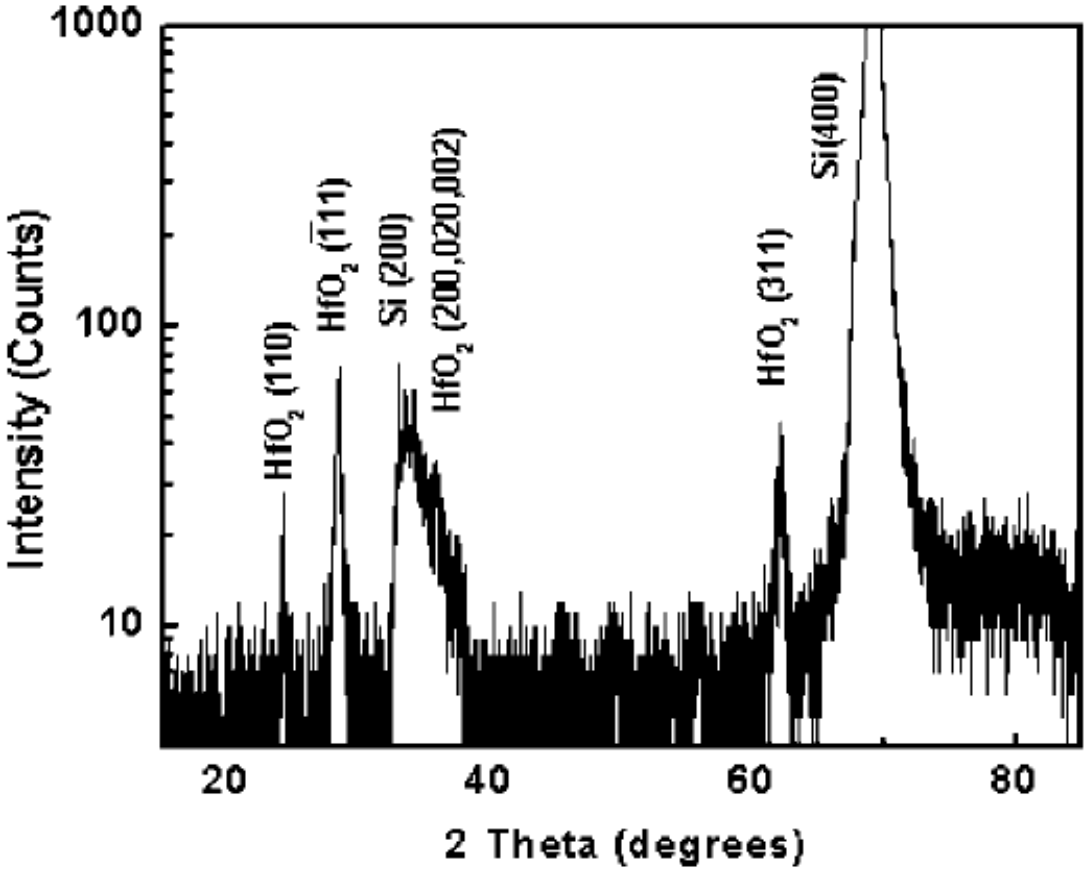

FIG. 5. 1 XRD pattern of a pure HfO_2 thin film.

High resolution transmission electron microscopy images (Fig.5.2) show a columnar structure in the HfO_2 films, and the film thickness is typically in the range of 200 nm. The thickness is also confirmed by Rutherford backscattering spectrometry (RBS). RBS results also showed no impurity in the thin films, and this is also confirmed by EDS analysis.

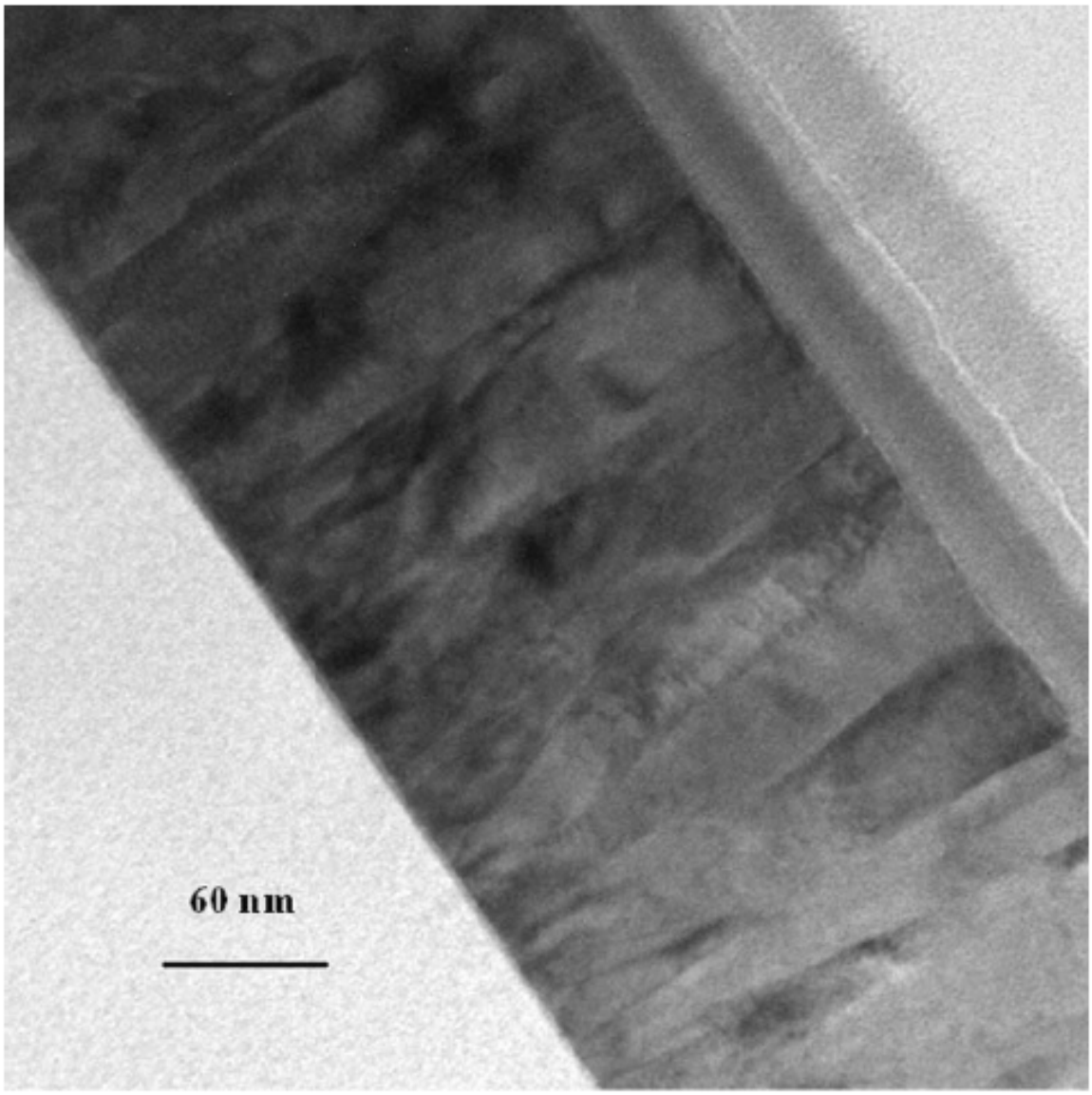

FIG.5.2 HREM image of the pure HfO2 thin film.

5.2.3 Magnetic Properties

Fig. 5.3 shows that the thin film is ferromagnetic at 300 K and 5 K for the pure HfO_2 (pureness 99.95%) film deposit on Si substrate. The magnitude of the observed magnetic moments is in the order of 10^{-6} emu. Fig. 5.4 show magnetization anisotropy of the thin film, which is approximately tripled when the magnetic field is applied perpendicularly to the plane of the thin film than applied in parallel, and this agrees with the result of Venkatesan et al.[1]

The anisotropy discussed above (Fig. 5.4), with magnetic field applied perpendicular and parallel to the thin film, was measured by inserting a 5×3 mm film sample into the measuring plastic straw. Two holes were cut on the straw to hold the sample in place. To investigate this further, we have measured the film with "complete" plastic straw (without two cuts). The results suggest the straw with holes itself introduces the "anisotropy". The M-H curves of the straw with holes, in the absence of a film, show a weak magnetic signal of 10^{-6} emu.

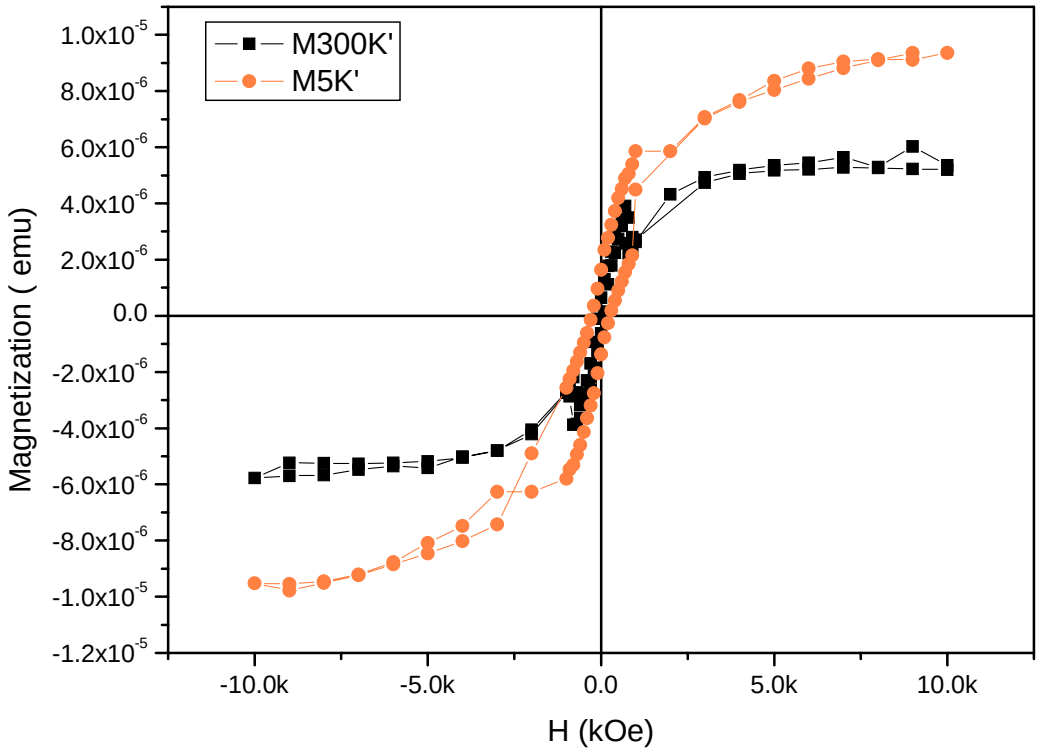

Fig. 5.3 the [*M* (*H*)] curves taken at 300 K and 5 K showing hysteresis loops

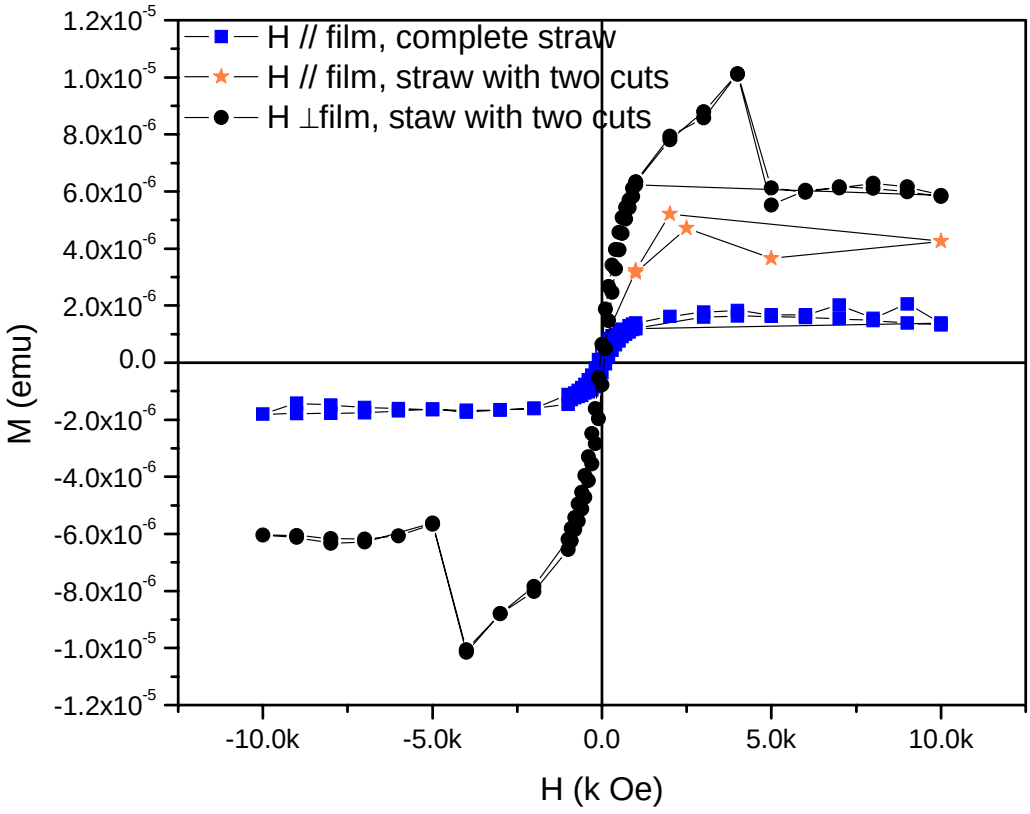

Fig. 5.4 magnetization of the thin film anisotropy

5.2.4 Signals From The Substrates

The method normally employed to measure the magnetic signal from the thin film is to subtract the signal of substrate from that which combines the substrate and thin film. Fig. 5.5 is the magnetization curve of Al_2O_3 substrate alone, which shows that the substrate itself has a magnetic signal comparable to our HfO_2 thin film on the Al_2O_3 substrate. This casts doubt on the accuracy of the measurement results presented earlier. After washing the same substrate with

acid, the magnetization curve (Fig. 5.6) showed a dramatic decrease in the magnetic signals, from 10^{-5} emu down to 10^{-7} emu, which confirmed that there were magnetic impurities on the substrate. A similar signal difference before and after the acid wash was also confirmed for Si substrates. Thereafter, all substrates for deposition were cleaned in strong acid (HCl: HNO3~3:1) for 20 h to get rid of the magnetic impurities.

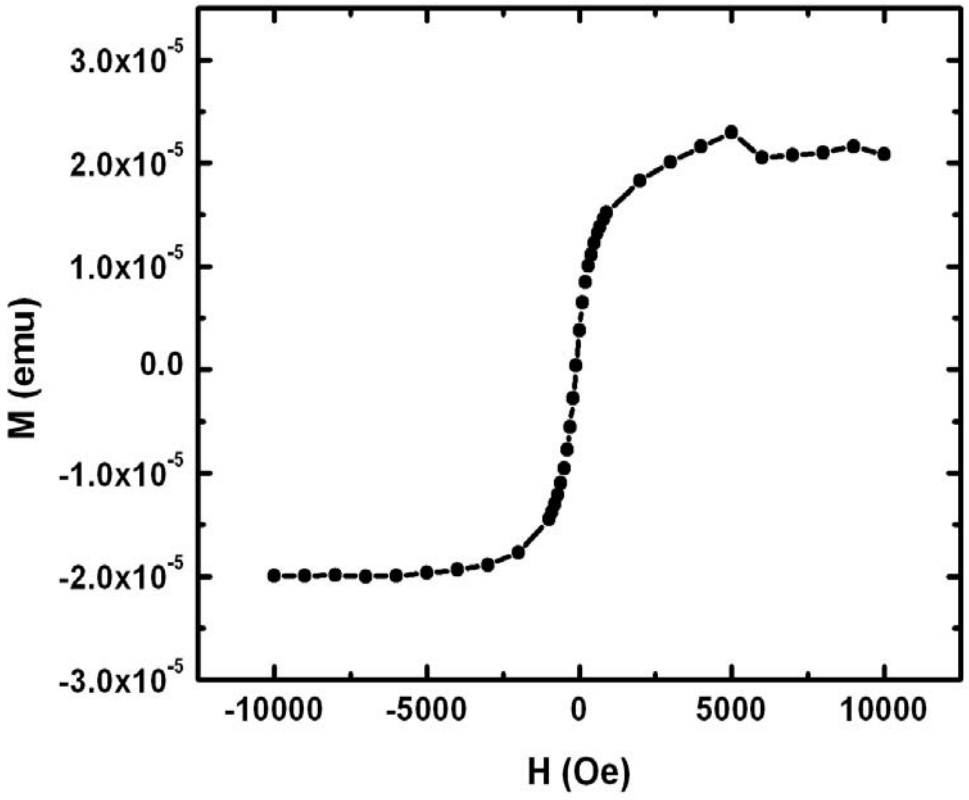

Fig. 5.5 Magnetization of Al_2O_3 substrate

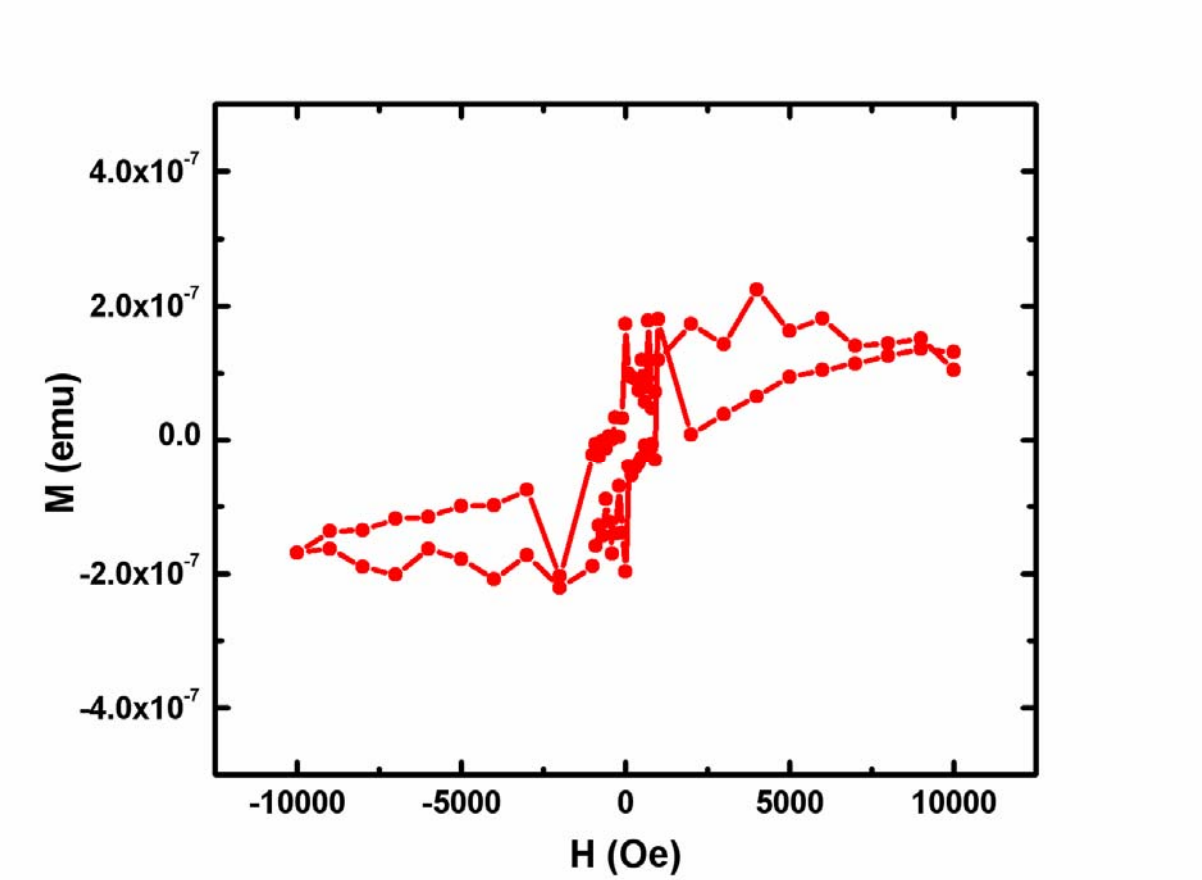

Fig. 5.6 Al_2O_3 substrate with acid wash.

HfO_2 powder of purity 99.95% is not the purest available, and the most likely impurity is ZrO_2. ZrO_2 thin film was deposited on the Si substrate under the same conditions as HfO_2. Fig. 5.7 shows the weak magnetic signal at 10^{-6} emu, which is in the same order of magnitude as the thin film shown in Fig. 5.4. The above data do not suggest ZrO_2 is ferromagnetic, rather they hint at the potential common source of the contamination.

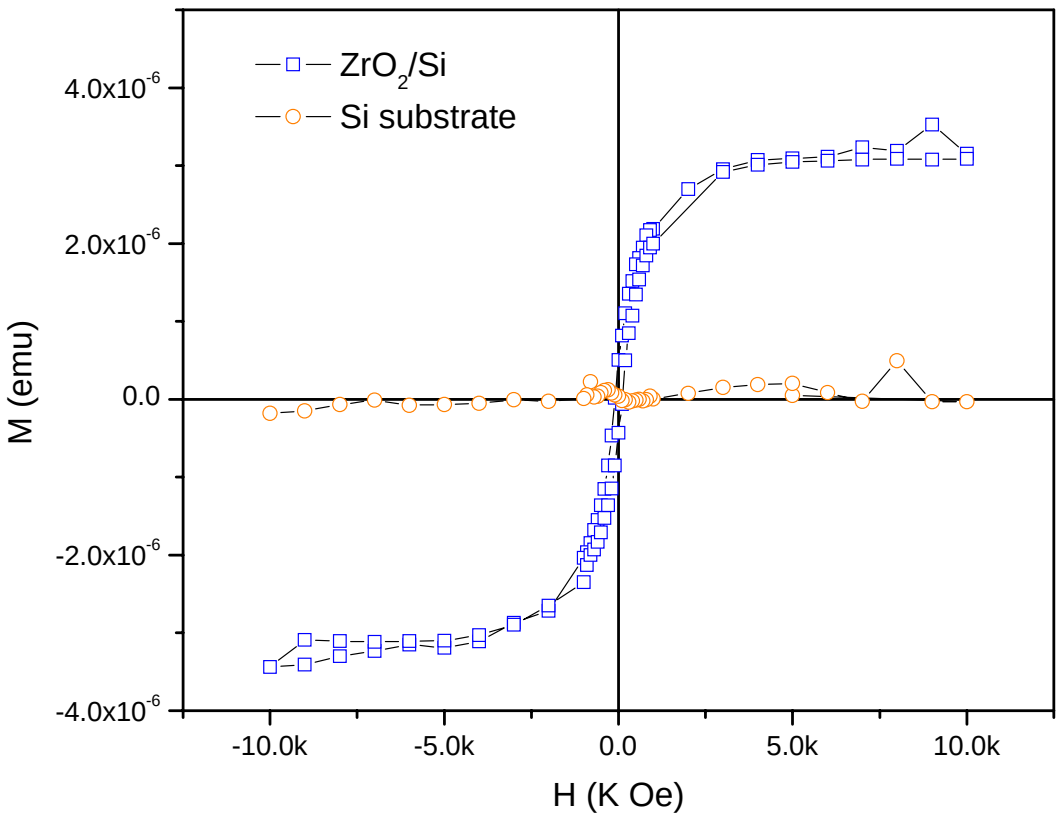

Fig. 5.7 Magnetic properties of ZrO_2 thin film on the SiO_2 substrate

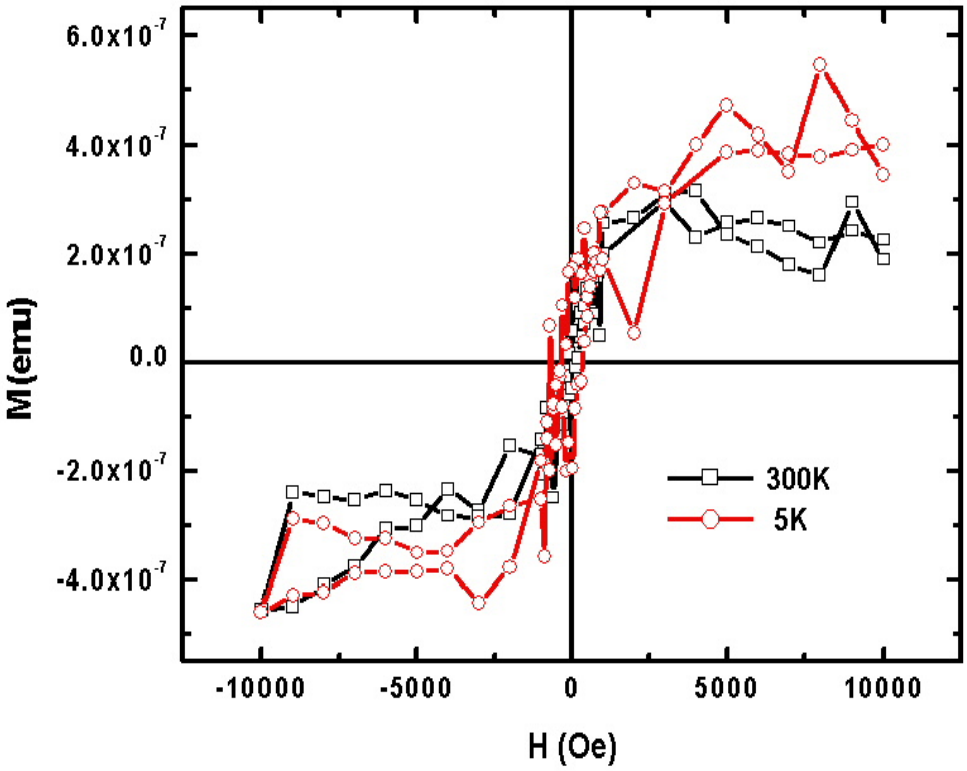

Fig. 5.8 The magnetization curves measured at 300 and 5 K for the purer HfO_2 (purity: 99.995%) film on Si substrate.

The effect of the purity of the raw HfO_2 was investigated. Figure 5.8 shows the magnetization curves measured at 300 and 5 K for films made of purer HfO_2 (purity = 99.995%) grown on Si substrate. An extremely weak ferromagnetic signal of about 5×10^{-7} emu was observed. If we assume that the measured signal is attributed to the HfO_2 films, the moment of the film is approximately equivalent to 0.0003 Bohr magneton per Hf ion, an extremely small

value. Moreover, considering the contribution from either the impurities in the target material or the residual impurities on the substrates, we conclude that our as-deposited HfO_2 films itself are not ferromagnetic.

The possible effects of defects/oxygen vacancies were studied on an as-deposited HfO_2 films by annealing it in air at 1000 ^oC, in an attempt to change the amount of oxygen vacancies. As shown in Fig. 5.9, no visible changes in the magnitude of the magnetization was seen. The mechanism for magnetism in these thin films appears not intimately connected to the defects or oxygen vacancies. Our study described above suggests that one needs to be extremely careful when drawing conclusions based on weak magnetic signals as low as 10^{-6}emu.

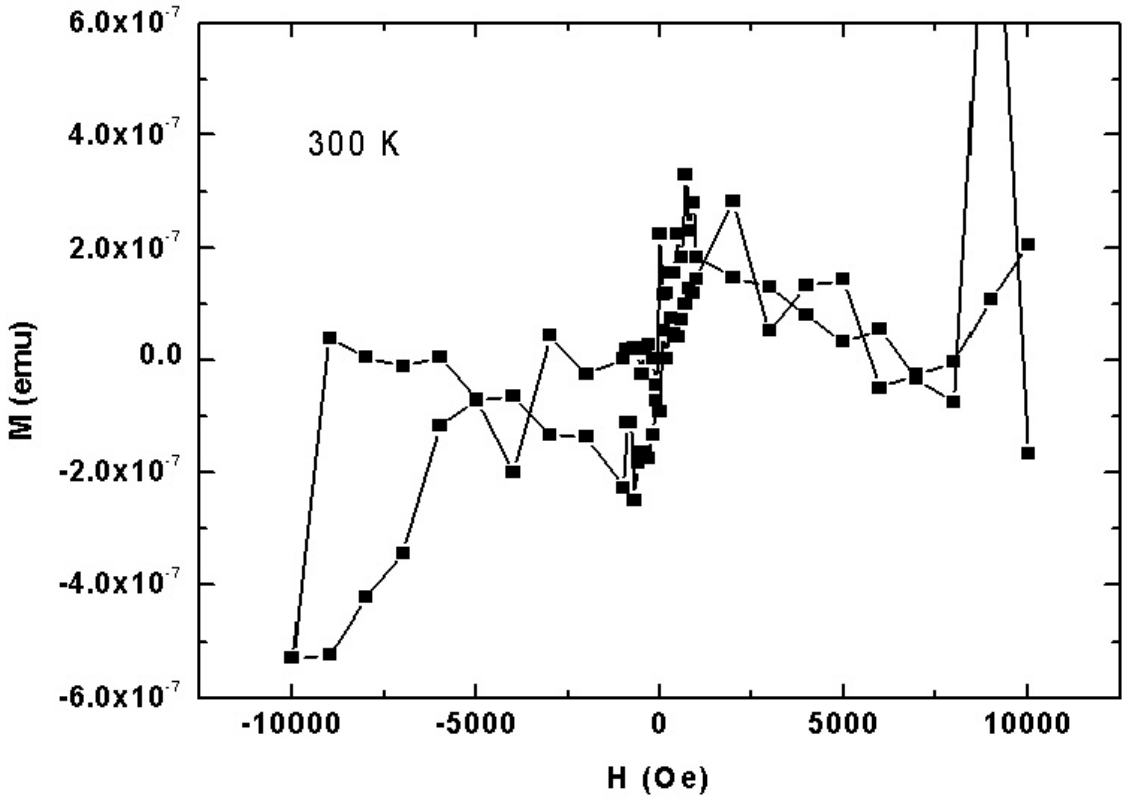

Fig. 5.9 Magnetization for HfO_2 film grown on Al_2O_3 annealed at 1000 ^oC.

5.3 Gd Doped HfO_2 Thin Film

As a wide band gap dielectric material with nonmagnetic $4f^{14}.5d^2.6s^2$ configuration, HfO_2 itself contributes no net moment. Theoretically, the medium of exchange by small amounts of impurity of the 4f band structure leads to 4f to 5d intra-atomic hybridization, and overlap with the unoccupied band structure just above the Fermi level, which may result in net overall magnetization. [54] Therefore, Gd (electrical outer shell structure $4f^7.5d^1.6s^2$), which have

relatively large magnetic moment among the rare earth elements, was chosen as the impurity to be doped in our HfO_2 thin film.

Fig. 5.10 is the XRD pattern of a Gd doped HfO_2 thin film deposited on Si (400) substrate. Other than the Si peaks from the substrate, all peaks match those of the simple monoclinic phase of HfO_2. Gd-doped HfO_2 thin films have the same XRD pattern except that their diffraction peaks have a small shift toward lower angles. For example, (111) peak is shifted by 0.18° from 28.29° to 28.11°, which means that the lattice parameter increases after the Gd doping. The ionic radii of ionized Gd (Gd^{3+}) are 0.1078 nm (six coordinate) and 0.1193 nm (eight coordinate), whereas the ionic radii of Hf^{4+} are 0.085 and 0.097 nm for the corresponding coordinates. Since the radii of Gd^{3+} are larger than those of Hf^{4+}, our XRD result implies that Gd dissolves in HfO_2 substitutionally.

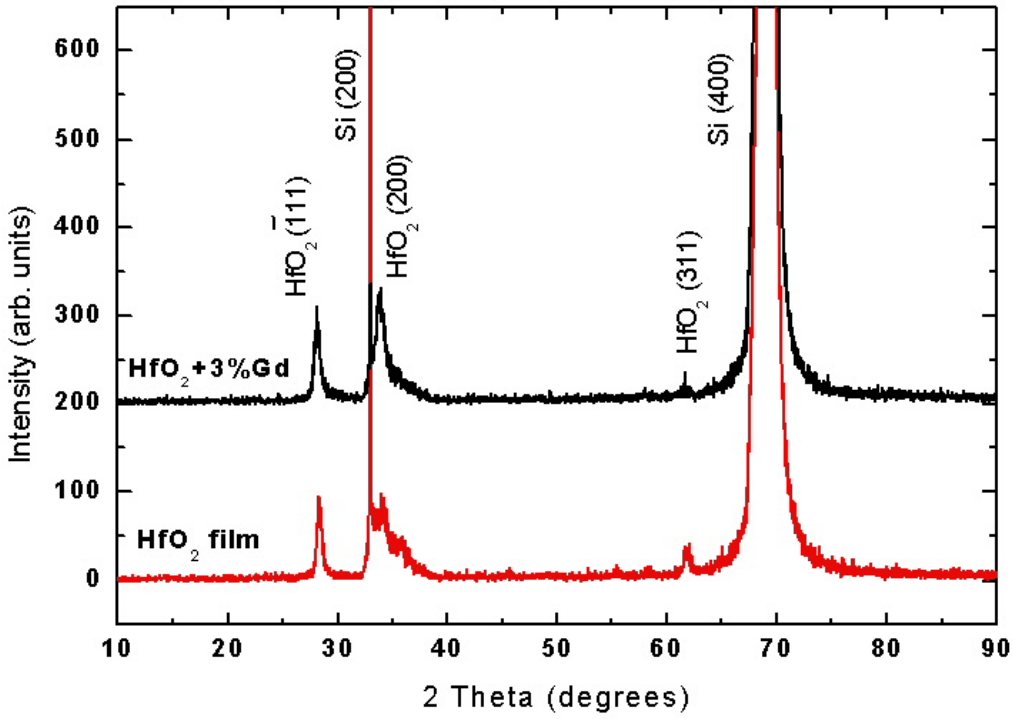

Fig. 5. 10 XRD patterns of a pure and Gd-doped HfO_2 thin film.

The film exhibits obvious paramagnetic signal, instead of ferromagnetic behaviour, in low temperature as shown in ZFC-FC curves (as shown in Fig. 5.11 a).

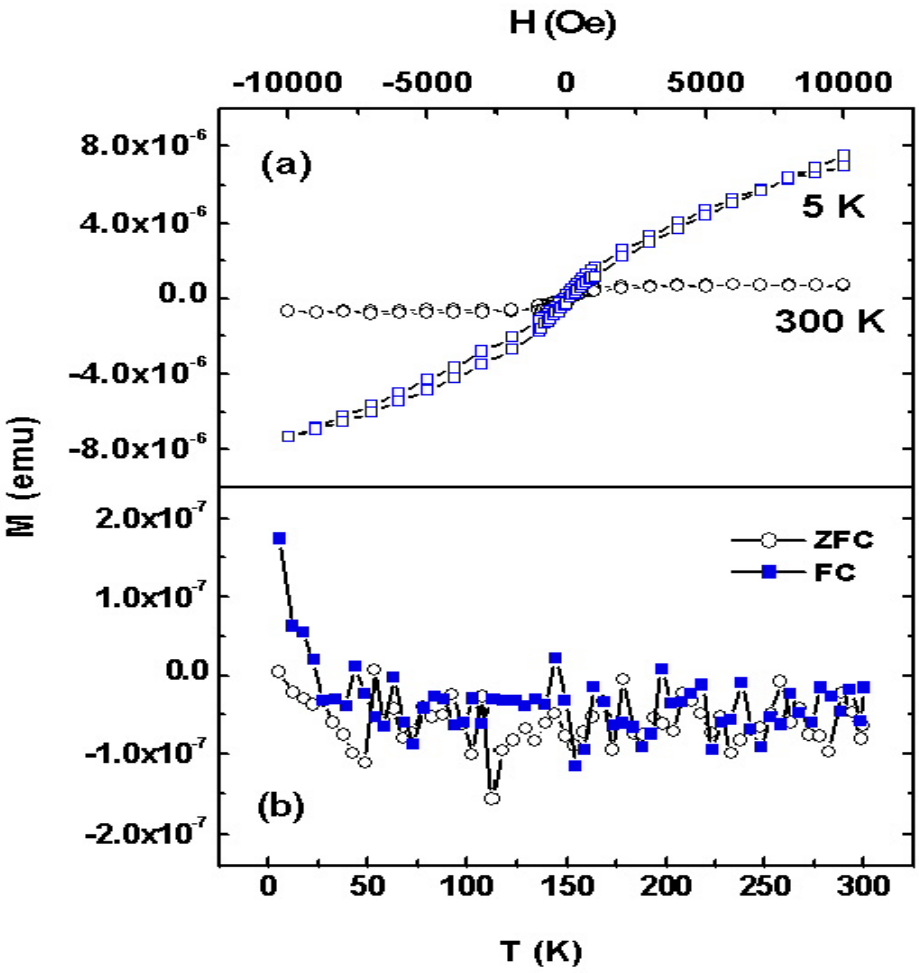

Fig. 5.11 (a) The magnetization curves at 300 and 5 K.

(b) ZFC-FC curves (H=100 One) for 3 at% Gd-doped HfO_2 thin film.

5.4 Defects Hypnosis

5.4.1 HfO_2 Thin Film

Different substrates should result in different interfaces and defect structures at the interfaces between the thin film and substrate, which may be the source of the ferromagnetism.[4,55] In order to alter the interface structure between the film and substrate, HfO_2 films were deposited on Al_2O_3 (012) and $LaAlO_3$ (100) substrates in addition to Si substrate. Our experiments (shown in Fig. 5.12) suggest no obvious difference in the magnetic properties of the HfO_2 films deposited on three different substrates (please also refer to Fig. 5.3 and Fig. 5.5).

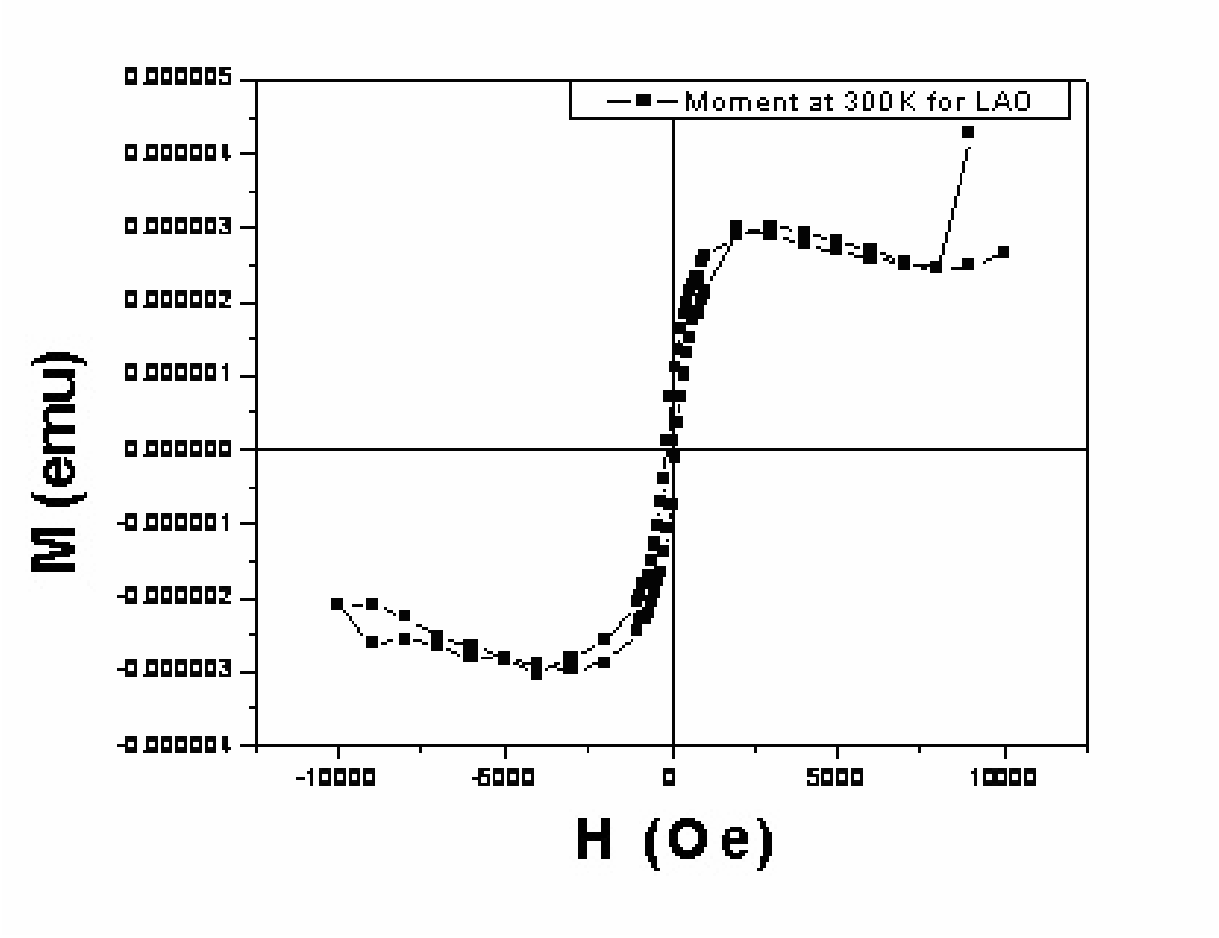

Fig. 5.12 Magnetization curve for HfO_2 film grown on LAO

All thin films were annealed in air at 700, 900, and 1000 °C to determine if annealing might change the defects in the HfO_2 films and influence their magnetic behaviour. In otherwise nonmagnetic compound such as CaB_6 and CaO, like HfO_2, the magnetism is considered to be driven by intrinsic point defects. However, the magnetic signal observed did not change with annealing or with temperature.

HfO_2 films were also deposited at room temperature in order to vary the defect density in the films. The films were found to be amorphous by XRD measurements. The magnetic signal was extremely weak, in the magnitude of 10^{-6} emu.

5.4.2 HfO_2 Powder

In addition to the films, HfO_2 powders of different purity were annealed at different temperature (700, 900, and 1100 °C) and in different atmospheres. XRD measurement indicates that there is no phase change for the HfO_2 powders after annealing under different atmospheres (shown in Fig. 5.13). Magnetic measurements show that neither the original powders nor annealed ones are ferromagnetic. The defects introduced by hydrogen reduction carried out here did not affect the magnetic behaviour of the powders, as shown in Fig. 5.14 and 5.15.

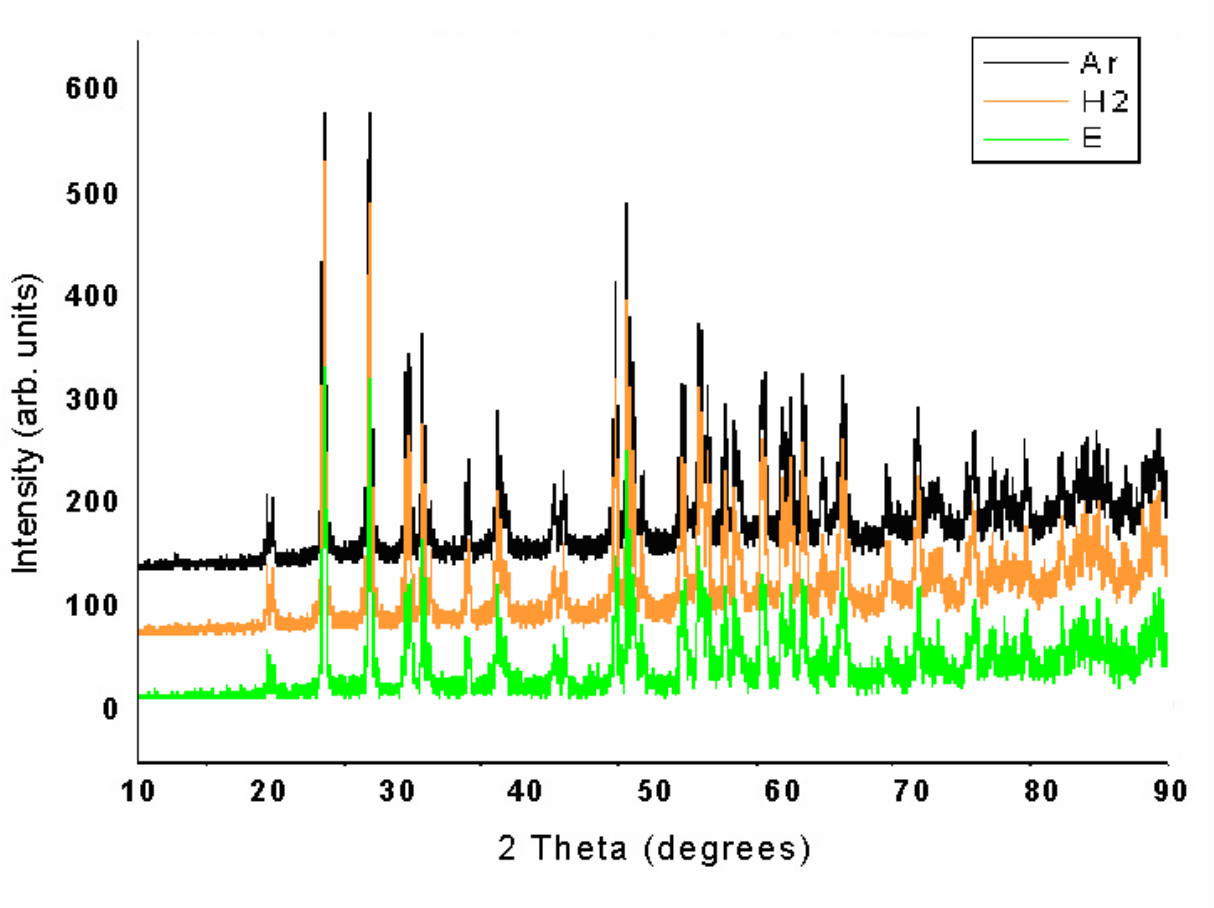

Fig. 5. 13 XRD measurements for the HfO_2 powders before (E-) and after annealing at Ar and H_2 atmosphere

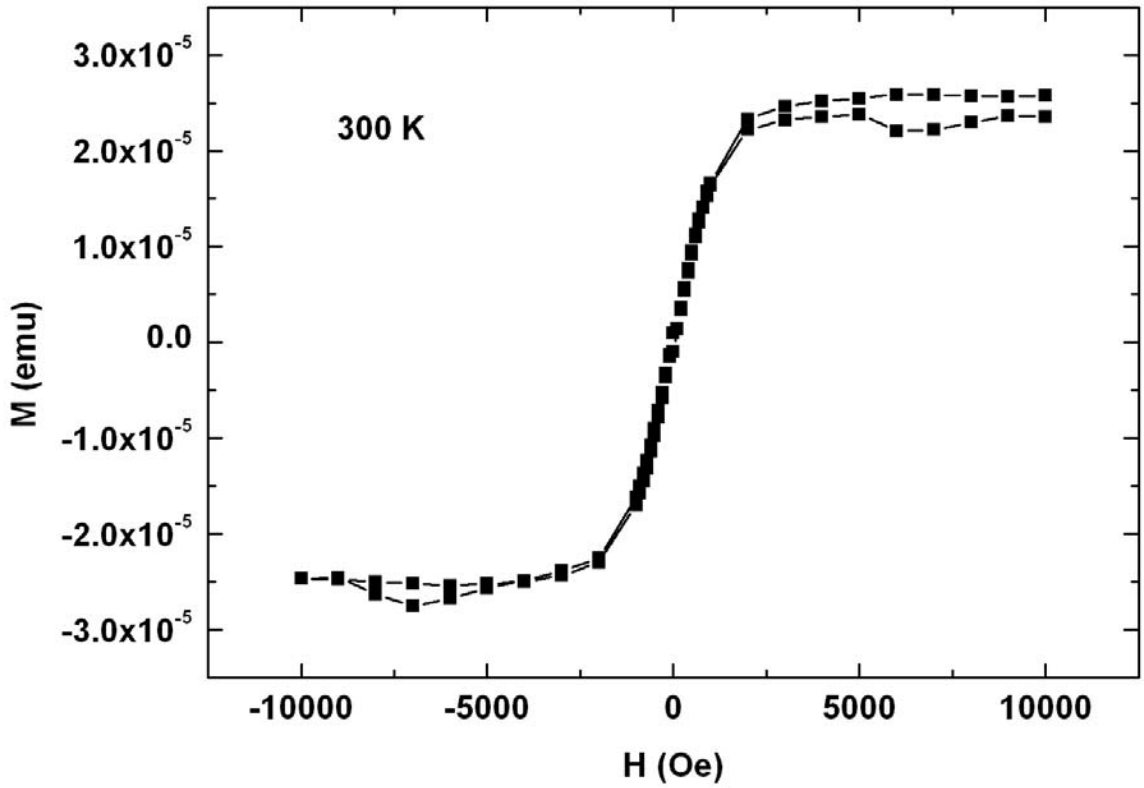

Fig. 5. 14 Magnetization curve for 99.95% HfO2 power

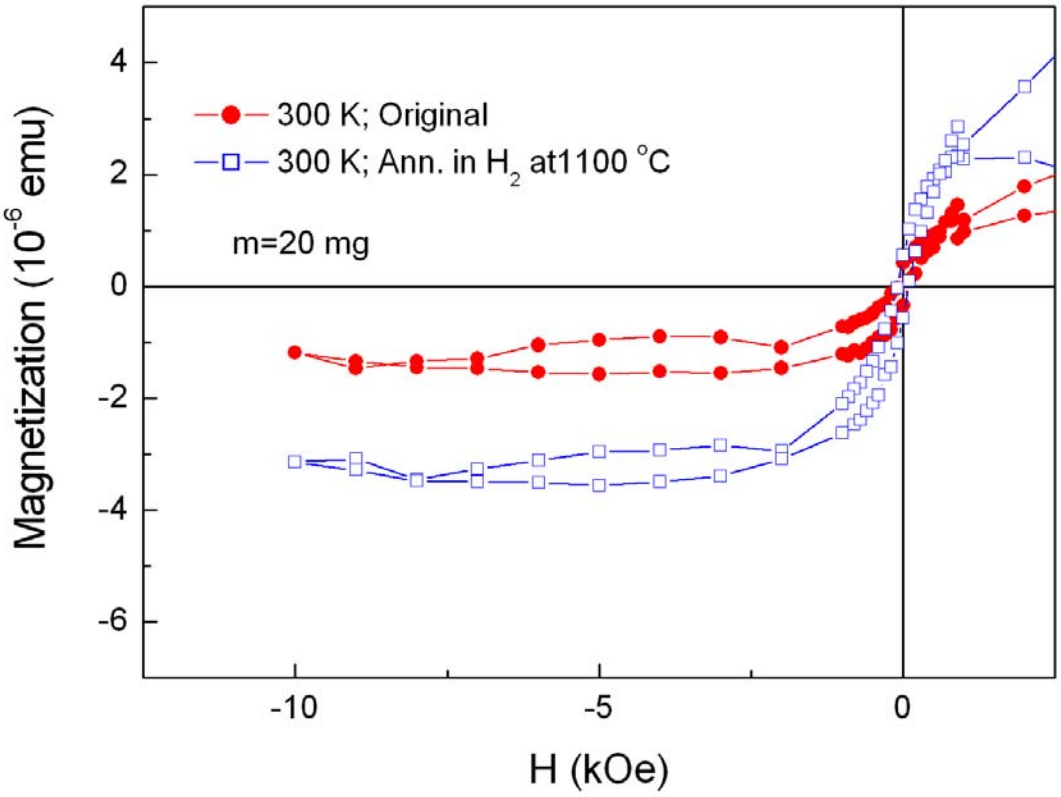

Fig. 5.15 Magnetization curves for 99.995% HfO2 power.

5.5 Conclusion

Our HfO_2 films deposited on Si (400), Al_2O_3 (012) and $LaAlO_3$ (100) substrates by PLD do not exhibit ferromagnetic properties, which is different from some of the reported data. The magnetic signal of the HfO_2 films does not change significantly with annealing at various temperatures and in different reducing atmospheres. HfO_2 powders (with and without annealing

in H_2 flow) are not ferromagnetic. For Gd-doped (3%) HfO_2 film, XRD result implies that Gd dissolves in HfO_2. The film exhibits paramagnetic signal at low temperature. ZFC-FC curves do not show ferromagnetic behaviour.

REFERENCES

[1] Sankar Das Sarma American Scientist , Volume: 89 Number: 6 Page: 516
[2] Germany (DE 3820475), Europe (0346817), USA (4,949,039).
[3] http://en.wikipedia.org/wiki/Giant_magnetoresistive_effect
[4] http://www.hitachigst.com/hdd/technolo/gmr/gmr.htm
[5] http://www.patentstorm.us/patents/6731477-fulltext.html
[6] J. S. Moodera, L. R. Kinder, T. M. Wong, and R. Meservey, Phys. Rev. Lett. **74**, 3273 (1995)
[7] http://www.patentstorm.us/patents/6218718-fulltext.html
[8] D.D. Awschalom and J.M. Kikkawa, Physics Today 52, 33 (1999).
[9] H. Ohno, in Semiconductor Spintronics and Quantum Computation, edited by D.D. Awschalom, N. Samarth, and D. Loss, (Springer, New York, 2002), p1.
[10] SCIENCE VOL 294 16 NOVEMBER 2001
[11] J M D Coey and S Sanvito, J. Phys. D: Appl. Phys. 37 (2004) 988–993, RES
[12] Ohno, Science 281 (14), 951 1998
[13] Edmonds et al. Phys. Rev. Lett. 92, 037201 (2004)
[14]WPrellier, A Fouchet and B Mercey, J. Phys.: Condens. Matter 15 (2003) R1583–R1601
[15] Matsumoto Y, Murakami M, Shono T, Hasegawa T, Fukumara T, Kawasaki M, Ahmet P, Chikyow T, Koshihara S Y and Koinuma H 2001 Science 291 854
[16] http://www.tkk.fi/Units/AES/projects/prlaser/thesis/node1.html
[17] http://mdpl.snu.ac.kr/facility.htm
[18] http://www.betelco.com/sb/phd/ch5/index.html
[19] http://www.biologie.uni-hamburg.de/b-online/e03/03e.htm
[20] WPrellier, A Fouchet and B Mercey, J. Phys.: Condens. Matter **15** (2003) R1583–R1601
[21] S. Duhalde, PHYSICAL REVIEW B **72**, 161313_R_ _2005.
[22] Wang Zhenjun,Wang Wendong,Tang Jinke. Appl.Phys.Lett.,2003,83(3):518～520.
[23] J.-Y. Kim, J.-H. Park, B.-G. Park, H.-J. Noh, S.-J. Oh, J. S. Yang, D.-H. Kim, S. D. Bu, T.-W. Noh, H.-J. Lin, H.-H. Hsieh, and C. T. Chen, PRL 2003 Jan 10;90(1):017401
[24] Kim JY, Park JH, Park BG, Noh HJ, Oh SJ, Yang JS, Kim DH, Bu SD, Noh TW, Lin HJ, Hsieh HH,Chen CT. Phys Rev Lett. 2003 Jan 10;90(1):017401.
[25] Origins of Coexistence of Conductivity and Transparency in SnO_2,
[26] Kimura H, Fukumura T, Koinuma H and Kawasaki M 2001 *Physica* E **10** 265
Kimura H, Fukumura T, Kawasaki M, Inaba K, Hasegawa T and Koinuma H 2002 *Appl. Phys. Lett.* 80 94
[27] D and Bakas T 2004 *J. Appl. Phys.* 95 7390
[28] C. B. Fitzgerald, M. Venkatesan, A. P. Douvalis, S. Huber, J. M. D. Coey and T. Bakas, J. Appl. Phys. 95, 7390
(2004)
[29] Fitzgerald C B, Venkatesan M, Douvalis A P, Huber S, Coey J M D and Bakas T 2004 *J. Appl. Phys.* 95 7390
[30] Coey J M D, Douvalis A P, Fitzgerald C B and Venkatesan M 2004 *Appl. Phys. Lett.* **84** 1332

[31] S. B. Ogale, R. J. Choudhary, J. P. Buban, S. E. Lofland, S. R. Shinde, S. N. Kale, V. N. Kulkarni, J. Higgins, C. Lanci, J. R. Simpson, N. D. Browning, S. Das Sarma, H. D. Drew, R. L. Greene, and T. Venkatesan, Phys. Rev. Lett. 91, 077205 (2003)
[32] N. H. Hong, J. Sakai, W. Prellier, and A. Hassini, J. Phys.: Condens. Matter **17**, 1697 (2005)
[33] Coey J M D, Douvalis A P, Fitzgerald C B and Venkatesan M 2004 *Appl. Phys. Lett.* **84** 1332
[34] Nguyen Hoa Hong, Antoine Ruyter1, W Prellier, Joe Sakai and
Ngo Thu Huong, J. Phys.: Condens. Matter 17 (2005) 6533–6538
[35] John Philip, Nikoleta Theodoropoulou, Geetha Berera, Jagadeesh S. Moodera and Biswarup Satpati, Appl. Phys. Lett. 85, 777 (2004).
[36] Y. W. Heo, J. Kelly, D. P. Norton, A. F. Hebard, S. J. Pearton, J. M. Zavada, and L. A. Boatner, Electrochem. Solid-State Lett. 7, G309 (2004)
[37] http://www.hpcc.nectec.or.th/wiki/index.php/Defect_band_structure_of_SnO_2
[38] S. A. Chambers and R. F. C. Farrow, MRS Bull. 28, 729 (2003)

[40] Nguyen Hoa Hong, Joe Sakai, Ngo Thu Huong, Nathalie Poirot,Antoine Ruyter, Phys. Rev. B 72, 045336 (2005)
[41] J. M. D. Coey, A. P. Douvalis, C. B. Fitzgerald, and M. Venkatesan, Appl. Phys. Lett. **84**, 1332 (2004).
[42] Hong, Nguyen Hoa; Poirot, Nathalie; Sakai, Joe, Applied Physics Letters, Volume 89, Issue 4, id. 042503 (3 pages) (2006)

[43] J. M. D. Coey, M. Venkatesan, P. Stamenov, C. B. Fitzgerald, and L. S. Dorneles, Phys. Rev. B **72**, 024450 (2005)

[44] Nguyen Hoa Hong, physica status solidi (c) Volume 4, Issue 3 , Pages 1270 - 1275

[45] M. Venkatesan, C. B. Fitzgerald, and J. M.D. Coey, Nature (London) 430, 630 (2004).
[46] T. Terashima, C. Terakura, Y. Umeda, N. Kimura, H. Aoki, and S. Kunii, J. Phys. Soc. Jpn. 69, 2423 (2000).
[47] D.P. Young, D. Hall, M.E. Torelli, Z. Fisk, J.D. Thompson, H.R. Ott, S.B. Oseroff, R.G. Goodrich, and R. Zysler, Nature (London) 397, 412 (1999)
[48] D.P. Young, Z. Fisk, J.D. Thompson, H.R. Ott, S.B. Oseroff, R.G. Goodrich, Nature (London) 420, 144 (2002).
[49] L. S. Dorneles, M. Venkatesan, M. Moliner, J. G. Lunney, and J. M. D. Coey, Appl. Phys. Lett. 85, 6377 (2004).
[50] I. S. Elfimov, S. Yunoki, and G. A. Sawatzky, Phys. Rev. Lett. 89, 216403 (2002).
[51] G. Bouzerar and T. Ziman, Phys. Rev. Lett. 96, 207602 2006
[52] Hongming Weng and Jinming Dong Physical Review B 73 132410 (2006)
[53] J. M. D. Coey, M. Venkatesan, P. Stamenov, C. B. Fitzgerald, and L. S. Dorneles, Phys. Rev. B 72, 024450 (2005)
[54] LOSOVYJ Ya. B. ; JINKE TANG ; WENDONG WANG ; YUANJIA HONG ; PALSHIN Vadim ; TITTSWORTH Roland, Physics Letters A, Volume 357, Issue 3, p. 240-244
[55] J. M. D. Coey, J. Appl. Phys. 97, 10D313 (2005)

VITA

Yuanjia Hong was born in ChangChun, Jilin Province, P.R. China. She graduated from Jilin University in 1996, she further continued to improve her education in Microelectronics and Solid State Electronics, and receive a master degree from ChangChun Institute of Optic and Fine Mechanics, ChangChun, China in April 2000. She become a PhD candidate in Key Laboratory of Rare Earth Chemistry and Physics, Changchun Institute of Applied Chemistry, Chinese Academy of Sciences, ChangChun, P.R. China in Spetember, 2000. Since 2002, she participated in research concerning magnetic electronic oxide materials as a research assistant in the Department of Physics at the University of New Orleans, and pursuing her PhD degree in Engineering and Appled Science.